PROOF COVER SHEET

Journal acronym:	TJRT
Author(s):	A. Innocenti, L. Marini, E. Meli, G. Pallini and A. Rindi
Article title:	Prediction of wheel and rail profile wear on complex railway networks
Article no:	897792
Enclosures:	1) Query sheet 2) Article proofs

Dear Author,

1. Please check these proofs carefully. It is the responsibility of the corresponding author to check these and approve or amend them. A second proof is not normally provided. Taylor & Francis cannot be held responsible for uncorrected errors, even if introduced during the production process. Once your corrections have been added to the article, it will be considered ready for publication.

Please limit changes at this stage to the correction of errors. You should not make trivial changes, improve prose style, add new material, or delete existing material at this stage. You may be charged if your corrections are excessive (we would not expect corrections to exceed 30 changes).

For detailed guidance on how to check your proofs, please paste this address into a new browser window: http://journalauthors.tandf.co.uk/production/checkingproofs.asp

Your PDF proof file has been enabled so that you can comment on the proof directly using Adobe Acrobat. If you wish to do this, please save the file to your hard disk first. For further information on marking corrections using Acrobat, please paste this address into a new browser window: http://journalauthors.tandf.co.uk/production/acrobat.asp

2. Please review the table of contributors below and confirm that the first and last names are structured correctly and that the authors are listed in the correct order of contribution. This check is to ensure that your name will appear correctly online and when the article is indexed.

Sequence	Prefix	Given name(s)	Surname	Suffix
1		A.	Innocenti	
2		L.	Marini	
3		E.	Meli	
4		G.	Pallini	
5		A.	Rindi	

Queries are marked in the margins of the proofs, and you can also click the hyperlinks below.

AUTHOR QUERIES

General points:

1. **Permissions:** You have warranted that you have secured the necessary written permission from the appropriate copyright owner for the reproduction of any text, illustration, or other material in your article. Please see http://journalauthors.tandf.co.uk/permissions/usingThirdPartyMaterial.asp.
2. **Third-party content:** If there is third-party content in your article, please check that the rightsholder details for re-use are shown correctly.
3. **Affiliation:** The corresponding author is responsible for ensuring that address and email details are correct for all the co-authors. Affiliations given in the article should be the affiliation at the time the research was conducted. Please see http://journalauthors.tandf.co.uk/preparation/writing.asp.
4. **Funding:** Was your research for this article funded by a funding agency? If so, please insert 'This work was supported by <insert the name of the funding agency in full>', followed by the grant number in square brackets '[grant number xxxx]'.
5. **Supplemental data and underlying research materials:** Do you wish to include the location of the underlying research materials (e.g. data, samples or models) for your article? If so, please insert this sentence before the reference section: 'The underlying research materials for this article can be accessed at <full link> / description of location [author to complete]'. If your article includes supplemental data, the link will also be provided in this paragraph. See <http://journalauthors.tandf.co.uk/preparation/multimedia.asp> for further explanation of supplemental data and underlying research materials.

AQ1 Please spell out "RFI" in full (if needed).

AQ2 Since "ρ(rho;)" has been defined as the material density, as per the definition, ρ = mass/volume, so the unit should be kg/m^3. Please clarify if the unit of "ρ" should be "kg/m^3" instead of "kg/m".

AQ3 Please check and confirm if the edits made to the sentence, "In the next Sections 5.1.1. ... 501 Minetto" convey the intended meaning or amend change if necessary.

AQ4 The intended sense of the sentence, "According to these quotas... the vehicle" is not clear. Please check that it reads correctly and supply a revised version if needed.

AQ5 Please note that the calculation is not defined for the "third rail step", but has been defined for "first, second, fourth and fifth rail steps." Please clarify whether it should be added or leave as is.

AQ6 Please check and confirm if the edit made to the sentence "The amount of ... tonnage)" conveys the intended meaning or amend if needed.

AQ7 Please confirm that the edit made to the sentence “The reference dimension... e = 10% conveys the intended meaning or amend change if needed.

AQ8 Please confirm whether the edit made to the sentence “By analysing the data...” conveys the intended meaning or else amend if needed.

AQ9 Please confirm if the edit made to the sentence “In conclusion, the innovative... data” conveys the intended meaning or amend if needed.

How to make corrections to your proofs using Adobe Acrobat/Reader

Taylor & Francis offers you a choice of options to help you make corrections to your proofs. Your PDF proof file has been enabled so that you can edit the proof directly using Adobe Acrobat/Reader. This is the simplest and best way for you to ensure that your corrections will be incorporated. If you wish to do this, please follow these instructions:

1. Save the file to your hard disk.

2. Check which version of Adobe Acrobat/Reader you have on your computer. You can do this by clicking on the "Help" tab, and then "About".

If Adobe Reader is not installed, you can get the latest version free from http://get.adobe.com/reader/.

3. If you have Adobe Acrobat/Reader 10 or a later version, click on the "Comment" link at the right-hand side to view the Comments pane.

4. You can then select any text and mark it up for deletion or replacement, or insert new text as needed. Please note that these will clearly be displayed in the Comments pane and secondary annotation is not needed to draw attention to your corrections. If you need to include new sections of text, it is also possible to add a comment to the proofs. To do this, use the Sticky Note tool in the task bar. Please also see our FAQs here: http://journalauthors.tandf.co.uk/production/index.asp.

5. Make sure that you save the file when you close the document before uploading it to CATS using the "Upload File" button on the online correction form. If you have more than one file, please zip them together and then upload the zip file.

If you prefer, you can make your corrections using the CATS online correction form.

Troubleshooting

Acrobat help: http://helpx.adobe.com/acrobat.html
Reader help: http://helpx.adobe.com/reader.html

Please note that full user guides for earlier versions of these programs are available from the Adobe Help pages by clicking on the link "Previous versions" under the "Help and tutorials" heading from the relevant link above. Commenting functionality is available from Adobe Reader 8.0 onwards and from Adobe Acrobat 7.0 onwards.

Firefox users: Firefox's inbuilt PDF Viewer is set to the default; please see the following for instructions on how to use this and download the PDF to your hard drive: http://support.mozilla.org/en-US/kb/view-pdf-files-firefox-without-downloading-them#w_using-a-pdf-reader-plugin

International Journal of Rail Transportation, 2014
Vol. 00, No. 00, 1–35, http://dx.doi.org/10.1080/23248378.2014.897792

Taylor & Francis
Taylor & Francis Group

Prediction of wheel and rail profile wear on complex railway networks

A. Innocenti, L. Marini, E. Meli*, G. Pallini and A. Rindi

Department of Industrial Engineering, University of Florence, via S. Marta n. 3, 50139 Firenze, Italy

(*Received 20 November 2013; accepted 12 February 2014*)

The modelling and the reduction of wear due to wheel-rail contact represents a crucial issue in railway applications, mainly correlated to safety, maintenance interventions and definition of strategies aimed at wheel profile optimization. A model for evaluating wheel and rail profile evolution due to wear developed for complex railway networks is presented in this paper. The model layout is composed of two mutually interacting but separate parts: a vehicle model (composed of multibody model and global contact model) for the dynamical simulations and a unit for wear computation (composed of the local contact model, the wear evaluation procedure and the profile update strategy). In order to achieve general significant accuracy results in reasonable computational effort, a suitable statistical approach for the railway track description is used, aimed at studying complex railway lines: in fact, the exhaustive analysis of vehicle dynamics and wear evolution on all the railway network is too expensive in terms of computational time for each practical purpose. The wear model has been validated in collaboration with Trenitalia S.P.A and RFI, which have provided technical documentation and experimental data relative to some tests performed on a environment exhibiting serious problems in terms of wear: the vehicle ALn 501 Minuetto operated on the Aosta-Pre Saint Didier Italian line.

Keywords: wheel-rail wear; multibody modelling of railway vehicles; statistical track analysis; wheel and rail profiles; complex railway network

1. Introduction

In the present research activity, the authors introduce a procedure to evaluate the evolution of the wheel and rail profiles due to wear expressly developed for complex railway networks. The general layout of the model consists of two mutually interactive subparts: the vehicle model (multibody model and 3D global contact model) and the wear model (local contact model, wear evaluation and profiles update) (see Figure 1). The multibody model accurately reproduces the dynamical characteristics of the investigated vehicle, considering all the significant degrees of freedom. The 3D global contact model has been developed by the authors in previous works [1,2] and it is employed to compute the wheel-rail contact points thanks to an innovative algorithm, which is established on suitable semi-analytic procedures, and then, for each contact point, to calculate the contact forces through Hertz's and Kalker's theory [3–5]. Since the new contact model is characterized by a high numerical efficency, the two models interact online during the analysis of the vehicle dynamics.

The part for the wear estimation is based on a local contact model (Kalker's FASTSIM algorithm is adopted [3,4]) and on an experimental relationship for the calculation of the

*Corresponding author. Email: enrico.meli@unifi.it

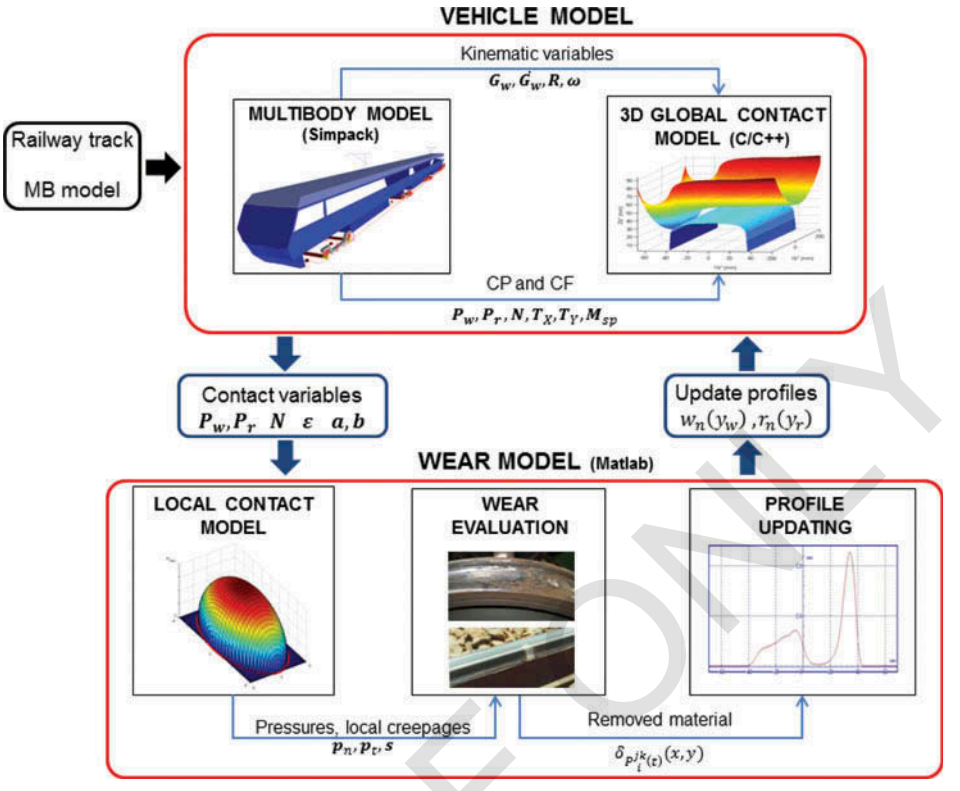

Figure 1. General architecture of the model.

removed material [6]. Starting from the vehicle model outputs (contact points, contact forces and global creepages), the wear model computes the overall quantity of worn material and its distribution along the wheel and rail profiles. The removal of material is performed according to the different time scales characterizing wheel and rail wear evolution.

Several interesting approaches dealing with wear models, based on both global and local models, can be found in the literature. In the global approach, generally used by commercial multibody software to reduce the computational load disregarding the model accuracy [7,8], wear is evaluated without neglecting the geometry of the contact area and hypothesizing that the contact between the surfaces takes place in a single point; such an approach may lead to both underestimation and overestimation of the worn material. The local approaches [7,9–18], instead, split the contact patch into adhesion and creep area, improving the accuracy of the results with a consequent increase of the computational load; some researches assessing the differences between global and local wear approaches can be found in literature [19].

However, in the study of complex railway networks, especially if local approaches to wear evaluation are adopted, several difficulties may be found to reach a good compromise between model accuracy and numerical efficiency. In this case, the computational load needed to carry out the exhaustive simulation of vehicle dynamics and wear evaluation turns out to be absolutely too high for each practical purpose.

To overcome the main critical aspect of wear evaluation models, the authors use a track statistical approach aimed at getting relevant results in a reasonable time; more specifically the authors suggest to substitute the railway network to be investigated with a discrete set of N_c different curved tracks (classified by radius, super-elevation and travelling speed) statistically equivalent to the entire network. In the previous years, many important research works concerning the statistical railway network description can be found in the literature, with the aim of reducing the computational effort required for the wear evaluation [6,9–12,19,20]. These works have been very helpful to the authors as starting point for the development of their statistical track approach. The adopted approach implies a significant reduction of the computational effort and, simultaneously, assures a good compromise in terms of model accuracy.

The current activity has been performed in collaboration with Trenitalia S.p.A. and RFI that have provided the experimental data regarding the Aosta-Pre Saint Didier railway line and the vehicle ALSTOM *DMU Aln 501 Minuetto* (which is affected by serious problems in terms of wear when operated in the above-mentioned railway line) needed for the preliminary validation of the model.

2. General architecture of the model

The general architecture of the model developed for studying the wear phenomena on complex railway lines is shown in the block diagram in Figure 1 in which two different main parts are present: the *vehicle model* necessary to perform the dynamical analysis and the *wear model*.

The *vehicle model* consists of the multibody model of the benchmark railway vehicle and the 3D global contact model that, during the dynamical simulation, interact directly online creating a loop. At each time integration step, the first one evaluates the kinematic variables (position, orientation and their derivatives) relative to the wheelsets and consequently to each wheel – rail contact pair. At this point, starting from the kinematic quantities the *wear model* calculates the global contact variables (contact points and contact forces, contact areas and global creepages). The 3D global contact model is based on both an innovative algorithm for the detection of the contact points (developed by the authors in previous works [1,2]) and Hertz's and Kalker's global theories for the evaluation of the contact forces [3]. The global contact variables are then passed to the multibody model to carry on the vehicle dynamics simulation.

The main inputs of the *vehicle model* are the multibody model of the railway vehicle and the corresponding railway track, represented in this work by the ALSTOM *DMU Aln 501 Minuetto* and the Aosta-Pre Saint Didier line, respectively (a critical scenario in Italian Railways in terms both of wear and stability).

The *wear model* is the part of the procedure concerning the prediction of the amount of worn material to be removed from the wheel and rail surfaces and is made up of three distinct phases: the local contact model, the wear evaluation and the profile update. The local contact model (based on both Hertz's local theory and simplified Kalker's algorithm FASTSIM [3,4]), starting from the global contact variables, estimates the local contact stresses and creepages inside the contact patch and detects the creep zone of the contact area. Subsequently the distribution of removed material is calculated both on the wheel and on the rail surface only within the creep area by using an experimental relationship between the removal

material and the energy dissipated by friction at the contact interface [6]. Finally the wheel and rail worn profiles are derived from the original ones through an appropriate updated strategy. The new updated wheel and rail profiles (one mean profile both for all the wheels of the vehicle and for all the considered tracks) are then fed back as inputs to the *vehicle model*, and the whole model architecture can proceed with the next discrete step. In particular, since the new wear model is conceived to describe complex railway networks (composed by several different tracks travelled by different vehicles), it is natural to consider, at this step, the wear evolution of a mean profile both for wheel and rail without distinguishing the single wheels and the single tracks.

For the sake of clarity, all the adopted work hypotheses have been summarized in the following:

- Discrete approach to study the wheel and rail profile evolutions due to wear, using an innovative update procedure to evaluate the simultaneous wear progress on both profiles (evolving on different time scales);
- Treatment of the complex railway network with statistical approach based on N_c classes of curves characterized by uniform intervals (both for the radius and for the superelevation);
- The effect of the transition sections has been considered (both in terms of lengths and contact point positions), but it has been equally distributed on the two adjacent full curves;
- To make up both for the deficiency of experimental data (relative to the reference quotas FT, FH, QR) and to reduce measurement errors, the evolution of a mean wheel profile for each vehicle has been considered.
- To make up for the lack of rail experimental data, the evolution of a mean rail profile for each class of curves (equal both for the inner and the outer side) has been considered; moreover an heuristic criteria found in literature [21] that considers the rail head wear (the QM reference quota) has been taken into account.
- The wear model has been validated on a quite tortuous line travelled by a vehicle that exhibits serious wear problem in such scenery (especially in terms of flange wear) and, consequently, considering a low travelled distance. This choice has been made to have significant results from a wear viewpoint in relatively few kilometres travelled by the vehicle. This way more manageable experimental campaigns characterized by reasonable measurement times have been obtained;
- The analysis has always been performed under dry contact conditions and without lubrication of the wheel and rail surfaces (constant and uniform friction all over the line);
- The experimental campaign has been carried out with only three identical Aln 501 Minuetto vehicles operating on the Aosta Pre Saint Didier network;
- The considered vehicles were initially equipped with new ORE S 1002 wheel profiles. At the same time, the initial rail profiles of the line were new UIC 60 profiles canted at $\alpha_p = 1/20$;
- The calculation of the removed material distributions due to wear is carried out according to the authors in Ref [6];
- The profiles update procedure makes use of linear filters to erase the numerical noise (naturally the effect of these filters has to be as limited as possible not to alter the removed material distributions).

3. The vehicle model

In this section, a brief description of the *vehicle model* is given. First of all, the multibody model of the studied benchmark vehicle is introduced; then the 3D global contact model is explained.

3.1. *The multibody model*

The benchmark vehicle investigated for this research is the *DMU Aln 501 Minuetto*, a passenger transport unit widespread in Italian Railways where is equipped with the standard ORE S1002 wheel profile and running on the UIC60 rail profile canted at 1/20 rad. This particular vehicle exhibits in fact severe wear and stability problems mainly caused by the adopted matching. Its mechanical structure and inertial, elastic and damping properties can be found in the literature [22–24]. Table 1 shows the main characteristics of the considered vehicle.

In Table 2, the inertia properties of the vehicle are shown: motors and gear boxes have not been modelled, and their inertia properties have been included in the motor bogie and in the motor wheelset (indicated in Table 2 with Bogie m, and Wheelset m, respectively) in order to take into account their different influence on the unsprung and sprung mass. The multibody model has been realized in the Simpack Rail environment and consists of 31 rigid bodies:

- three coaches;
- four bogies: the intermediate ones, interposed between two successive coaches, are trailer bogies while the other ones are motor bogies;
- eight wheelsets: two for each bogie; and
- sixteen axleboxes: two for each wheelset.

Table 1. Main characteristics of the Aln 501 Minuetto DMU.

Length	51.9 m
Width	2.95 m
Height	3.82 m
Bogie pivot distances	14.8–13.8–14.8 m
Bogie wheelbase	2.80 m
Unladen weight	100 t
Wheel arrangement	Bo-2-2-Bo
Wheel diameter	850 mm
Max. speed	130 km/h

Table 2. Inertia properties of the multibody model.

MBS body	Mass (kg)	Roll inertia (kg m^2)	Pitch inertia (kg m^2)	Yaw inertia (kg m^2)
Coach M	31,568	66,700	764,000	743,000
Coach T	14,496	30,600	245,000	236,000
Bogie m	3306	1578	2772	4200
Bogie t	3122	1674	3453	5011
Wheelset m	2091	1073	120	1073
Wheelset t	1462	1027	120	1027

The rigid bodies are connected by means of appropriate elastic and damping elements; particularly the vehicle is equipped with two suspension stages. The primary suspensions connect the wheelsets to the bogies and comprise two springs and two vertical dampers, while the secondary suspensions connect the bogies to the coaches and comprise the following elements:

- two air springs;
- six non-linear dampers (lateral, vertical and anti - yaw dampers);
- one non-linear traction rod;
- the roll bar (not visible in the figure);
- two non-linear lateral bumpstops.

Both the stages of suspensions have been modelled by means of three-dimensional viscoelastic force elements taking into account all the mechanical non-linearities of the system (bumpstop clearance, dampers and rod behaviour). The main linear characteristics of the suspensions are shown in Table 3 while the non-linear characteristics are imposed as a function of displacement and velocity for the springs and the dampers, respectively.

3.2. *The global contact model*

In this research activity, a specifically developed 3D global contact model has been used in order to improve reliability and accuracy of the contact points detection, compared to those given by the Simpack Rail contact model. In particular, the adopted contact model is based on a two-step procedure; at the first step the contact points number and positions are determined through an innovative algorithm designed and validated by the authors in previous works [1,2,16]. During the second step, for each detected contact point, the global contact forces are evaluated using Hertz's and Kalker's global theories [3,5].

The algorithm for the contact points detection starts from the standard idea that the contact points make stationary the distance between the wheel and rail surfaces; in more details the distance has a point of relative minimum if there is no penetration between the considered surfaces, while it has a relative maximum in the other case. The main features of the innovative adopted algorithm, based on the reduction of the algebraic problem dimension from 4D to 1D, are the following:

Table 3. Main linear stiffness properties of the ALn 501 'Minuetto'.

Primary suspension	Flexicoil k_z	9.01×10^5 N/m
	Flexicoil k_x, k_y	1.26×10^6 N/m
	Sutuco bushing k_x	2.0×10^7 N/m
	Sutuco bushing k_y	1.5×10^7 N/m
Secondary suspension	Airspring k_z	3.98×10^5 N/m
	Airspring k_x, k_y	1.2×10^5 N/m
	Anti-roll bar k_α	2.6×10^6 N/rad
Coach connection	Bushing k_x, k_z	7.24×10^7 N/m
	Bushing k_y	5.2×10^6 N/m

- It is a fully 3D procedure that takes into account all the six relative degrees of freedom (DOF) between wheel and rail;
- It can support generic railway tracks and generic wheel and rail profiles;
- It assures a general and accurate treatment of the multiple contact without introducing simplifying assumptions on the problem geometry and kinematics and limits on the number of contact points detected;
- It assures high numerical efficiency making possible the online implementation within the commercial multibody software (Simpack–Rail, Adams–Rail) without discrete look-up tables; in this way also the numerical performances of the commercial multibody software are improved.

At this point, for each contact point detected, the global creepages ε acting in the contact patch and the normal N^r and tangential $\mathbf{T}^r$ contact forces are determined. The normal forces N^r are calculated by means of Hertz's theory [5] [25], while tangential contact forces $\tilde{T}_x^r$, $\tilde{T}_y^r$ and the spin torque M_{sp}^r are calculated by means of the Kalker's global theory [3].

4. The wear model

In this section, the three phases in which the wear model has been divided will be described in details: the local contact model, the evaluation of the amount of removed material and the wheel and rail profile update.

4.1. *The local contact model*

The inputs of the wear model are the global contact parameters estimated by the vehicle model. Since a local wear computation is required, the global contact parameters need to be post-processed and this can be achieved through the simplified Kalker's theory implemented in the FASTSIM algorithm. This theory starts from the global creepages (ε), the normal global forces N^r, the contact patch dimensions (a, b) and the material properties to compute the local distribution of normal p_n and tangential $\mathbf{p}_t$ stresses and local creepages $\mathbf{s}$ across the wheel-rail contact area. For a more detailed description of the FASTSIM algorithm, one can refer to the literature [26].

4.2. *The wear evaluation*

To evaluate the distribution of removed material on wheel and rail due to wear, an experimental relationship between the volume of removed material and the frictional work [6] has been used.

The adopted wear function employs the local normal p_n and tangential $\mathbf{p}_t$ stresses (expressed in $\mathrm{N/mm^2}$), the local creepages $\mathbf{s}$ (m/s) and the vehicle velocity V (m/s) as inputs to directly compute the volume of worn material $\delta_{P_{wi}^j(t)}(x,y)$ and $\delta_{P_{ri}^j(t)}(x,y)$ (where x and y indicate the coordinates of a generic point of the contact patch) related to the i-th contact points $P_{wi}^j(t)$ and $P_{ri}^j(t)$ on the j-th wheel and rail pair for unit of distance travelled by the vehicle (expressed in m) and for unit of surface (expressed in mm). More specifically, local contact stresses and creepages are used to evaluate the *wear index* I_W (expressed in $\mathrm{N/mm^2}$), which represents the frictional work (expressed in N m) per unit of contact area (expressed in $\mathrm{mm^2}$) and per unit of rolled distance (expressed in m):

$$I_W = \frac{\mathbf{p}_t \cdot \mathbf{s}}{V}. \tag{1}$$

This index can be correlated with the *wear rate* K_W, that is the mass of removed material (expressed in $\mu g/(mmm^2)$) for unit of distance travelled by the vehicle and for unit of surface. The correlation is based on real data available in literature [6], which have been acquired from experimental wear tests carried out in the case of metal to metal contact with dry surfaces using a twin disc test arrangement. The experimental relationship between K_W and I_W adopted for the wear model described in this work is the following:

$$K_W(I_W) = \begin{cases} 5.3 * I_W & I_W < 10.4 \\ 55.1 & 10.4 \leq I_W \leq 77.2. \\ 61.9 * I_W - 4778.7 & I_W > 77.2 \end{cases} \tag{2}$$

Once the wear rate $K_W(I_W)$ is known (the same both for the wheel and for the rail), the specific volume of removed material on the wheel and on the rail (for unit of distance travelled by the vehicle and for unit of surface) can be calculated as follows (expressed in $mm^3/(mmm^2)$):

$$\delta_{P^j_{wi}(t)}(x,y) = K_W(I_W)\frac{1}{\rho} \quad \delta_{P^j_{ri}(t)}(x,y) = K_W(I_W)\frac{1}{\rho} \tag{3}$$

where ρ is the material density (expressed in kg/m).

4.3. *The profile update procedure*

After obtaining the amount of worn material, wheel and rail profiles need to be updated to be used as the input of the next step of the whole model. The new profiles, denoted by $w_n(y_w)$ and $r_n(y_r)$, are computed from the old ones $w_o(y_w)$, $r_o(y_r)$ and from all the calculated distributions $\delta_{P^j_{wi}(t)}(x,y)$ and $\delta_{P^j_{ri}(t)}(x,y)$ of worn material through an appropriate set of numerical procedures that defines the update strategy.

The whole numerical procedure which computes the new profiles can be summed up in the following steps:

- *Longitudinal integration*:

$$\frac{1}{2\pi w(y^j_{\mathrm{wi}})}\int_{-a(y)}^{+a(y)} \delta_{P^j_{wi}(t)}(x,y)\mathrm{d}x = \delta^{tot}_{P^j_{wi}(t)}(y) \tag{4}$$

$$\frac{1}{l_{\mathrm{sim}}}\int_{-a(y)}^{+a(y)} \delta_{P^j_{ri}(t)}(x,y)\mathrm{d}x = \delta^{tot}_{P^j_{ri}(t)}(y) \tag{5}$$

where $a(y)$ is the longitudinal length of the contact patch (evaluated in y), $w(y^j_{\mathrm{wi}})$ is the wheel radius evaluated in y^j_{wi} and l_{sim} is the length of the simulated track (when the complete railway track of length l_{track} is simulated $l_{\mathrm{sim}} = l_{\mathrm{track}}$, while in the statistical analysis case $l_{\mathrm{sim}} = l_{\mathrm{ct}}$ with l_{ct} equal to the length of each of the N_{c} curved tracks).

- *Track integration*:

$$\int_{T_{\text{in}}}^{T_{\text{end}}} \delta^{\text{tot}}_{P^j_{\text{wi}}(t)}(y)V(t)\mathrm{d}t \approx \int_{T_{\text{in}}}^{T_{\text{end}}} \delta^{\text{tot}}_{P^j_{\text{wi}}(t)}(s_w - s^{cj}_{wi}(t))V(t)\mathrm{d}t = \Delta_{P^j_{wi}}(s_w) \tag{6}$$

$$\int_{T_{\text{in}}}^{T_{\text{end}}} \delta^{\text{tot}}_{P^j_{\text{ri}}(t)}(y)V(t)\mathrm{d}t \approx \int_{T_{\text{in}}}^{T_{\text{end}}} \delta^{\text{tot}}_{P^j_{\text{ri}}(t)}(s_r - s^{cj}_{ri}(t))V(t)\mathrm{d}t = \Delta_{P^j_{\text{ri}}}(s_r); \tag{7}$$

the track integration sums all the wear contributes of the dynamic simulation to obtain the depth of removed material for wheel $\Delta_{P^j_{wi}}(s_w)$ and rail $\Delta_{P^j_{ri}}(s_r)$ expressed in mm = mm^3/mm^2. The introduction of the natural abscissas s_w and s_r of the curves $w(y_w)$ and $r(y_r)$ leads to a better accuracy in the calculation of the worn profiles (the natural abscissas of the contact points s^{cj}_{wi} and s^{cj}_{wi} can be evaluated from their positions P^j_{wi} and P^j_{ri}).

- *Sum on the contact points*:

$$\sum\nolimits_{i=1}^{N_{PDC}} \Delta_{P^j_{\text{wi}}}(s_w) = \Delta^w_j(s_w) \quad \sum\nolimits_{i=1}^{N_{PDC}} \Delta_{P^j_{\text{ri}}}(s_r) = \Delta^r_j(s_r) \tag{8}$$

where N_{PDC} is the maximum number of contact points of each single wheel (and respectively of each single rail).

- *Average on the wheel-rail pairs*:

$$\frac{1}{N_w}\sum\nolimits_{j=1}^{N_w} \Delta^w_j(s_w) = \overline{\Delta}^w(s_w) \quad \frac{1}{N_w}\sum\nolimits_{j=1}^{N_w} \Delta^r_j(s_r) = \overline{\Delta}^r(s_r) \tag{9}$$

where N_w is the number of vehicle wheels.

- *Average on the curved tracks of the statistical approach*: this step of the update procedure is important when a statistical description of the track is adopted. In this case, different wear distributions $\overline{\Delta}^w_k(s_w)$ and $\overline{\Delta}^r_k(s_r)$ for each of the N_c curve classes will be obtained from the previous steps (with $1 \le k \le N_c$). At this point, the statistical weights of the curve classes p_k, calculated as the ratio between the track length characterized by the curve conditions related to the k-th class (in terms of radius and superelevation values) and the total railway track length, have to be introduced to consider the frequency with which each curve appears on the actual railway track. Consequently for the statistical approach, the following relationships hold:

$$\sum\nolimits_{k=1}^{N_c} p_k\overline{\Delta}^w_k(s_w) = \overline{\Delta}^w_{\text{stat}}(s_w) \quad \sum\nolimits_{k=1}^{N_c} p_k\overline{\Delta}^r_k(s_r) = \overline{\Delta}^r_{\text{stat}}(s_r) \tag{10}$$

with $\sum_{k=1}^{N_C} p_k = 1$ (see also Section 5.2). Obviously, when the dynamic simulations are performed on the complete railway track, Equation (10) simply becomes:

$$\overline{\Delta}^w(s_w) = \overline{\Delta}^w_{\text{track}}(s_w) \quad \overline{\Delta}^r(s_r) = \overline{\Delta}^r_{\text{track}}(s_r). \tag{11}$$

- *Scaling*: the almost linearity of the wear model inside the discrete steps km_{step} in which the total mileage travelled km_{tot} is subdivided is a working hypothesis coming from the discrete approach of the model. The linearity hypothesis is equivalent to suppose that the wear rate inside the simulated distance (km_{prove}) remains the same also inside the discrete step km_{step} (reasonable since the considered vehicle repeats the same railway track both during the simulated distance (km_{prove}) and during the discrete step (km_{step})).

The evaluation of the discrete steps, with the consequent scaling of $\overline{\Delta}^{w}_{\text{stat}}(s_w)$, $\overline{\Delta}^{w}_{\text{track}}(s_w)$ and $\overline{\Delta}^{r}_{\text{stat}}(s_r)$, $\overline{\Delta}^{r}_{\text{track}}(s_r)$, represents the major difference between the update strategy of wheel and rail:

(1) The removed material on the wheel due to wear is proportional to the distance travelled by the vehicle; in fact a point of the wheel is frequently in contact with the rail in a number of times proportional to the distance. The following nomenclature is introduced (see Figure 2):
   - km_{tot} is the total mileage travelled by the considered vehicle; its value can be chosen depending on the purpose of the simulations, for example, according to the wheelset maintenance European norm [27];
   - km_{step} is the length of the discrete step corresponding to the threshold value on the wear depth D^{w}_{step};
   - km_{prove} is the overall mileage travelled by the vehicle during the dynamic simulations. This parameter assumes a different value according to the different way in which the track is treated: if the wear evolution is evaluated on the overall railway track (of length l_{track}), then $km^{\text{track}}_{\text{prove}} = l_{\text{track}}$ while, if the track statistical approach is considered, $km^{\text{stat}}_{\text{prove}} = l_{\text{ct}}$ is the mileage travelled by the vehicle during each of the N_c dynamic simulations.

Finally, the material removed on the wheels and the corrensponding km_{step} value have to be scaled according to the following laws:

$$\overline{\Delta}^{w}_{\text{stat}}(s_w)\frac{D^{w}_{\text{step}}}{D^{w}_{\text{stat}}} = \overline{\Delta}^{w\ sc}_{\text{stat}}(s_w), \quad km^{\text{stat}}_{\text{step}} = \frac{D^{w}_{\text{step}}}{D^{w}_{\text{stat}}} km^{\text{stat}}_{\text{prove}} \tag{12}$$

$$\overline{\Delta}^{w}_{\text{track}}(s_w)\frac{D^{w}_{\text{step}}}{D^{w}_{\text{track}}} = \overline{\Delta}^{w\ sc}_{\text{track}}(s_w), \quad km^{\text{track}}_{\text{step}} = \frac{D^{w}_{\text{step}}}{D^{w}_{\text{track}}} km^{\text{track}}_{\text{prove}} \tag{13}$$

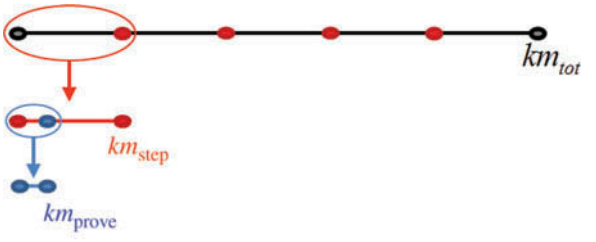

Figure 2. Discretization of the total mileage.

where:

$$D^{w}_{\text{stat}} = \max_{s_w} \overline{\Delta}^{w}_{\text{stat}}(s_w) \quad D^{w}_{\text{track}} = \max_{s_w} \overline{\Delta}^{w}_{\text{track}}(s_w). \tag{14}$$

(2) The depth of rail wear is not proportional to the distance travelled by the vehicle; in fact, the rail tends to wear out only in the zone where it is crossed by the vehicle and, increasing the travelled distance, the depth of removed material remains the same. On the other hand, the rail wear is proportional total tonnage M_{tot} burden on the rail and thus to the total vehicle number N_{tot} moving on the track. Therefore, if N_{step} is the vehicle number moving in a discrete step (corresponding to the threshold value on the wear depth Δ^{r}_{step}), the quantity of rail removed material at each step will be:

$$\overline{\Delta}^{r}_{\text{stat}}(s_r)\frac{D^{r}_{\text{step}}}{D^{r}_{\text{stat}}} = \overline{\Delta}^{r\ sc}_{\text{stat}}(s_r), \quad N^{\text{stat}}_{\text{step}} = \frac{D^{r}_{\text{step}}}{D^{r}_{\text{stat}}} N^{\text{stat}}_{\text{prove}} \tag{15}$$

$$\overline{\Delta}^{r}_{\text{track}}(s_r)\frac{D^{r}_{\text{step}}}{D^{r}_{\text{track}}} = \overline{\Delta}^{r\ sc}_{\text{track}}(s_r), \quad N^{\text{track}}_{\text{step}} = \frac{D^{r}_{\text{step}}}{D^{r}_{\text{track}}} N^{\text{track}}_{\text{prove}} \tag{16}$$

where $N^{\text{stat}}_{\text{prove}} = N_c$, obviously $N^{\text{track}}_{\text{prove}} = 1$ and:

$$D^{r}_{\text{stat}} = \max_{s_r} \overline{\Delta}^{r}_{\text{stat}}(s_r) \quad D^{r}_{\text{track}} = \max_{s_r} \overline{\Delta}^{r}_{\text{track}}(s_r). \tag{17}$$

- *Smoothing of the removed material*:

$$\Im\left[\overline{\Delta}^{w\ sc}_{\text{stat}}(s_w)\right] = \overline{\Delta}^{w\ sc}_{\text{stat}\ sm}(s_w), \quad \Im\left[\overline{\Delta}^{w\ sc}_{\text{track}}(s_w)\right] = \overline{\Delta}^{w\ sc}_{\text{track}\ sm}(s_w) \tag{18}$$

$$\Im\left[\overline{\Delta}^{r\ sc}_{\text{stat}}(s_r)\right] = \overline{\Delta}^{r\ sc}_{\text{stat}\ sm}(s_r), \quad \Im\left[\overline{\Delta}^{r\ sc}_{\text{track}}(s_r)\right] = \overline{\Delta}^{r\ sc}_{\text{track}\ sm}(s_r); \tag{19}$$

the numerical noise and short spatial wavelengths without physical meaning that affect the worn material distributions can be passed to the new profiles $\tilde{w}^{\text{stat}}_{n}(s_w)$, $\tilde{w}^{\text{track}}_{n}(s_w)$ and $\tilde{r}^{\text{stat}}_{n}(s_r)$, $\tilde{r}^{\text{track}}_{n}(s_r)$ with consequent problems raising in the global contact model. Hence, an appropriate smoothing of the worn material distributions is required. In this case, it is achieved by means of a first-order discrete filter (i.e. a moving average filter with window size equal to $1\% \div 5\%$ of the total number of points in which the profiles are discretized); obviously, the discrete filter has to conserve the mass.

- *Profile update:* the last step consists in the update of the old profiles $\tilde{w}^{\text{stat}}_{o}(s) = w^{\text{stat}}_{o}(y)$, $\tilde{w}^{\text{track}}_{o}(s) = w^{\text{track}}_{o}(y)$ and $\tilde{r}^{\text{stat}}_{o}(s_r) = r^{\text{stat}}_{o}(y_r)$, $\tilde{r}^{\text{track}}_{o}(s_r) = r^{\text{track}}_{o}(y_r)$ to obtain the new profiles $\tilde{w}^{\text{stat}}_{n}(s) = w^{\text{stat}}_{n}(y)$, $\tilde{w}^{\text{track}}_{n}(s) = w^{\text{track}}_{n}(y)$ and $\tilde{r}^{\text{stat}}_{n}(s_r) = r^{\text{stat}}_{n}(y_r)$, $\tilde{r}^{\text{track}}_{n}(s_r) = r^{\text{track}}_{n}(y_r)$; since the removal of material occurs in the normal direction to the profiles ($\mathbf{n}^{\mathbf{r}}_{\mathbf{w}}$ and $\mathbf{n}^{\mathbf{r}}_{\mathbf{r}}$ are the outgoing unit vectors for the wheel and rail profiles, respectively), once removed the quantities $\overline{\Delta}^{w\ sc}_{\text{stat}\ sm}(s_w)$, $\overline{\Delta}^{w\ sc}_{\text{track}\ sm}(s_w)$ and $\overline{\Delta}^{r\ sc}_{\text{stat}\ sm}(s_r)$, $\overline{\Delta}^{r\ sc}_{\text{track}\ sm}(s_r)$ a re-parameterization of the profiles is needed in order to obtain again curves parameterized by means of the curvilinear abscissa.

5. Railway track description

In this section, the two different strategies for the track description used in this work will be presented. In particular, initially the whole Aosta-Pre Saint Didier line will be introduced togheter with the experimental data provided by our industrial partners and related to the *DMU Aln 501 Minuetto* travelling on this track; then the statistical procedure used to extract the set of N_c curvilinear tracks will be described.

5.1. *The Aosta Pre Saint Didier line*

The whole Aosta-Pre Saint Didier railway network (characterized by an approximate length of $l_{\text{track}} \approx 31$ km) has been reconstructed and modelled in the Simpack environment starting from the track data. This is a very sharp track on the Italian Railways, and the scenery is rather interesting since the *DMU Aln 501 Minuetto* exhibits serious problems on this track in terms of wear, requiring frequent maintenance interventions on the wheelsets.

AQ3 In the next Sections 5.1.1 and 5.1.2, we shall discuss the experimental data consisting in the wear control parameters measured as a function of the total distance travelled by the *DMU Aln 501 Minuetto*.

5.1.1. *Wear control parameters*

The reference parameters FH, FT and QR are capable of estimating the wheel profile evolution due to wear without necessarily knowing the whole profile shape (see Figure 3).

AQ4 According to these quotas, the user will be able both to estabslished when the worn wheel profile will have to be re-profiled and to detect if the wear compromises the dynamical stability of the vehicle [27].

An additional control parameter is then introduced to evaluate the evolution of rail wear. Particularly the QM quota is defined as the rail head height in the point $y_r = 760$ mm with respect to the centre line of the track: this y_r value depends on the railway gauge (equal to 1435 mm in the Aosta-Pre Saint Didier line) and on the laying angle α_p of the track (equal to 1/20 rad). Physically the QM quota gives information on the rail head wear (see Figure 4).

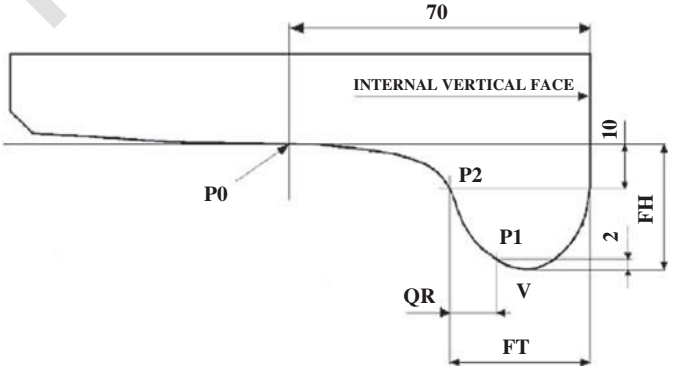

Figure 3. Definition of the wheel wear control parameters.

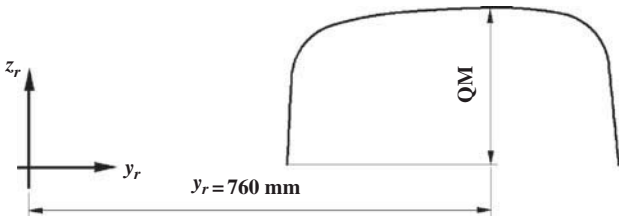

Figure 4. Definition of rail wear control parameters.

Even if the QM quota has a precise physical meaning (it gives information about the rail head wear), it is not thought to be measured through a real measurement procedure. The choice of this particular quantity is mainly due to the lack of experimental data concerning the rail wear during this initial phase of the research activity. (No direct measures of the rail head wear, the rail side wear and the complete rail profile are available.) More, in particular, the QM quota has been used to be compared to an heuristic criterion on the rail head wear found in the literature [21]; this way a preliminary model validation, in terms of rail wear, has been obtained.

5.1.2. *Experimental data*

The experimental data have been measured on three different vehicles *DMU Aln 501 Minuetto* operating on the Aosta-Pre Saint Didier track that are conventionally called DM061, DM068 and DM082. A mean value of the kinematic friction coefficient equal to $\mu_c = 0.28$ has been chosen (typical of the most frequent operating conditions).

The reference quota values have been measured for all the vehicle wheels (each vehicle has 8 wheelsets and thus 16 wheels as specified in Section 3.1). However, the following data processing has been necessary in order to obtain as output a single average wheel profile that could be effectively compared with the profile extracted from the numerical simulation and to reduce the measurement errors:

(1) Initially the arithmetic mean on all the 16 vehicle wheels has been evaluated; the mean is necessary to obtain a single wheel profile and, at the same time, to reduce the measurement errors affecting the experimental data;
(2) Then a scaling of the quota values has been carried out in order to delete the offset on the initial value of the considered quantities: this procedure imposes that all the wear control parameters start from their nominal values (the standard values for the new unworn ORE S 1002 profile have been used) in order to remove the initial differences among the vehicles due to measurement errors;
(3) The arithmetic mean on the three vehicles MD061, MD068, MD082 has not been carried out, in order to maintain a dispersion range for the experimental data.

The experimental data, properly processed, are summarized in Table 4. As can be seen, the flange height (FH) remains approximately constant because of the low mileage travelled by the vehicles, while the flange thickness FT and the flange steepness QR decrease almost linearly and highlight, according to the characteristics of the track, the wear concentration in the wheel flange.

Concerning the rail wear, the QM quota evolution is compared with a criterion present in the literature (based on the total tonnage burden on the track) [21]. Particularly a

Table 4. Experimental data processed.

Vehicle	Distance travelled (km)	FH (mm)	FT (mm)	QR (mm)
DM061	0	28.0	32.5	10.8
	1426	28.2	31.5	9.8
	2001	28.1	30.8	9.1
	2575	28.0	30.2	8.6
DM068	0	28.0	32.5	10.8
	1050	28.0	31.8	10.0
	2253	28.0	30.2	8.5
	2576	28.0	30.0	8.4
DM082	0	28.0	32.5	10.8
	852	28.0	32.3	10.6
	1800	28.0	31.3	9.6
	2802	28.0	30.3	8.7
	3537	27.6	30.0	8.3

proportionality relationship between tonnage and wear holds: a rail wear of 1 mm on the rail head height every 100 Mt (millions of tons) of accumulated tonnage.

It has to be noted that also the gauge corner rail wear is surely an important parameter to study the rail wear evolution (together with the rail head wear); in fact on the inner rail, the rail head wear is usually more relevant while on the outer one the gauge corner wear becomes prevalent. However, at this phase of the research activity, direct experimental measurements have been performed only on the wheel profiles (more simple to be carried out and managed) and not the rail profiles. Consequently, to overcome the deficiency of rail experimental data and perform a simple preliminary model validation of the rail wear behaviour, the authors decided to use only the previous heuristic criterion that approximately links the rail head wear (the quota QM) to the total tonnage burden on the track (and then to the total number of travelling vehicles).

5.2. *The statistical approach*

The present section is an overview on the procedure used in deriving a significant statistical track description, an essential task to make possible and rationalize the approach and the simulation work on a complex railway line, as it will be shown in the following by the comparison between the two track description strategies in terms of computational effort.

In the present work, the statistical approach has been exploited to draw up a virtual track of the Aosta-Pre Saint Didier line. The basic idea is to substitute the simulation on the whole track with an equivalent set of simulations on short curved tracks (in this research activity, the curved tracks length is equal to $l_{ct} = 200$ m). More precisely, the steps performed to get the statistical representation were the following:

- A set of n_{class} curve radius intervals characterized by a minimum R_{min} and a maximum R_{max} radius were identified by analysing the database;
- Each of these intervals was furthermore divided in n_{class} superelevation subclasses, each of them with its own h_{min} and h_{max};
- In this case, the same number n_{class} both for the radius and the superelevation classes is considered. By way of example in Table 5 is shown the statistical

Table 5. Data of the curvilinear tracks of the statistical analysis.

R_{min}(m)	R_{max}(m)	Superelevation $h_{min} - h_{max}$(mm)	R_c(m)	H (mm)	V (km/h)	p_k %
150	175	0–19	–			
		20–39	–			
		40–59	–			
		60–79	–			
		80–99	–			
		100–119	162	110	57	0.93
		120–140	162	131	60	1.30
175	209	0–19	–			
		20–39	–			
		40–59	–			
		60–79	–			
		80–99	195	90	60	7.09
		100–119	195	103	60	7.42
		120–140	195	126	60	5.48
209	259	0–19	–			
		20–39	–			
		40–59	–			
		60–79	237	70	60	0.87
		80–99	237	83	60	8.76
		100–119	237	109	60	4.63
		120–140	237	120	60	0.47
259	342	0–19	–			
		20–39	–			
		40–59	293	50	60	0.28
		60–79	293	65	60	3.05
		80–99	293	83	60	0.90
		100–119	293	100	60	0.31
		120–140	–			
342	503	0–19	–			
		20–39	–			
		40–59	376	49	60	1.13
		60–79	376	62	60	1.26
		80–99	–			
		100–119	–			
		120–140	–			
503	948	0–19	–			
		20–39	774	24	60	1.73
		40–59	774	40	60	0.42
		60–79	–			
		80–99	–			
		100–119	–			
		120–140	–			
948	8400	0–19	3572	5	60	2.40
		20–39	3572	20	60	0.91
		40–59	–			
		60–79	–			
		80–99	–			
		100–119	–			
		120–140	–			
8400	∞	0	∞	0	130	50.65

description related to $n_{\text{class}} = 7$ (at the radius classes has to be added the straight class);

- For each radius class, a representative radius R_c was calculated as a weighted average on all the curve radii, using the length of curve as a weighting factor;
- Likewise for each superelevation subclass, the correspondent representative superelevation H was chosen as a weighted average on all the curve superelevation, using the length of curve as a weighting factor;
- For each subclass, a speed value V was chosen as the minimum value between the maximum speed allowable in curve (equal to $V_{\max} = 60$ km/h and depending on the radius, the superelevation and the vehicle characteristics), and the speed $\tilde{V}$ calculated imposing a non-compensated acceleration of $a_{\text{nc}}^{\lim} = 0.8\text{m/s}^2$ [21] [22]:

$$\frac{\tilde{V}^2}{R_c} - \frac{H}{s} g = a_{\text{nc}}^{\lim} \qquad V = \min(\tilde{V}, V_{\max}). \tag{20}$$

For the straight class, the considered speed value, obtained from the track data, is equal to 130km/h;

- A weighting factor p_k, calculated as explained in Section 4.3, was introduced for each subclass to take into account the frequency of a certain matching radius-superelevation in the track and to diversify the wear contributions of the different curves;
- The transition lengths of the real track are incorporated in the constant curvature sections next to them: in particular, both the inner transition and the outer transition are divided in to two equal parts, and one half is included in the previous constant curvature section while the other half is included in the next one. Hence, the wear is numerically evaluated on curves and straight tracks only.

As an example in Table 5 is reported the track classification provided by the statistical approach to the Aosta-Pre Saint Didier line with $n_{\text{class}} = 7$, made up of $N_c = 30$ different classes (29 curves and the straight track). For each one of the N_c classes of curves, the unworn (i.e just re-profiled) UIC 60 rail profile canted at 1/20 has been adopted as starting condition for the wear evaluation (also the wheels start from the unworn condition).

6. Results

In this section, the simulation campaign carried out to study the wheel and rail wear evolution will be described. Then the results concerning both the complete railway track analysis and the statistical analysis approach will be compared in terms of efficiency and accuracy. Initially, the complete track results will be compared with the experimental data, then the comparison between the complete track results and the statistical analysis ones imposing a class number $n_{\text{class}} = 10$ will be performed, and finally the sensibility analysis of the statistical approach with respect to the n_{class} parameter will be presented.

6.1. *Simulation strategy*

As explained in Section 4.3, the wheel and rail wear evolutions evolve according to different time scales and a full simulation of such events would require a too heavy

computational effort. For this reason, the following specific algorithm has been adopted for updating the profiles:

(1) To have a good compromise between calculation times and result accuracy, a suitable number of discrete steps both for the wheel and for the rail steps have been chosen, $n_{sw} = 20$ and $n_{sr} = 5$ (this way an appreciable wear on the wheel and rail profiles has been obtained with a reasonable computational effort, considering the available computational resources; this is a critical aspect especially for the rail wear that is characterized by much greater time scales):
   (a) consequently the wheel wear threshold D^{w}_{step} (see Section 4.3) has been fixed equal to 0.2 mm;
   (b) the value of the rail wear threshold D^{r}_{step} (see Section 4.3) has been set equal to 0.8 mm to obtain an appreciable rail wear during the simulations.
(2) The wear evolutions on wheel and rail have been decoupled because of the different scales of magnitude:
   (a) while the wheel wear evolves, the rail is supposed to be constant: in fact, in the considered time scale, the rail wear variation is negligible;
   (b) the time scale characteristic of the rail wear evolution, much greater than the wheel wear evolution one, causes the same probability that each discrete rail profile comes in contact with each possible wheel profile. For this reason, for each rail profile, the whole wheel wear evolution (from the original profile to the final profile) has been simulated.

Based on the two previous hypotheses, the simulations have been carried out according to the following strategy:

Wheel profile evolution at first rail step: w_i^0

$$p_{1,1}\left\{(w_0^0\ r_0) \rightarrow (w_1^0\ r_0) \rightarrow \ldots \rightarrow (w_{n_{sw}-1}^0\ r_0) \rightarrow w_{n_{sw}}^0\right.$$

AQ5 **Average on the rails $r_1^{(i+1)}$ for the calculation of the second rail step:** r_1

$$p_{1,2}\left\{\begin{pmatrix} w_0^0 & r_0 \\ w_1^0 & r_0 \\ \vdots & \vdots \\ w_{n_{sw}-1}^0 & r_0 \end{pmatrix} \rightarrow \begin{pmatrix} r_1^{(1)} \\ r_1^{(2)} \\ \vdots \\ r_1^{(n_{sw})} \end{pmatrix} \rightarrow r_1\right.$$

Wheel profile evolution at fourth rail step: $w_i^{n_{sr}-1}$

$$p_{5,1}\left\{(w_0^{n_{sr}-1}\ r_{n_{sr}-1}) \rightarrow (w_1^{n_{sr}-1}\ r_{n_{sr}-1}) \rightarrow \ldots \rightarrow (w_{n_{sw}}^{n_{sr}-1}\ r_{n_{sr}-1}) \rightarrow w_{n_{sw}}^{n_{sr}-1}\right.$$

Average on the rails $r_{n_{sr}}^{(i+1)}$ for the calculation of the fifth rail step: $r_{n_{sr}}$

$$p_{n_{sr}}, 2\left\{\begin{pmatrix} w_0^{n_{sr}-1} & r_{n_{sr}-1} \\ w_1^{n_{sr}-1} & r_{n_{sr}-1} \\ \vdots & \vdots \\ w_{n_{sw}-1}^{n_{sr}-1} & r_{n_{sr}-1} \end{pmatrix} \rightarrow \begin{pmatrix} r_{n_{sr}}^{(1)} \\ r_{n_{sr}}^{(2)} \\ \vdots \\ r_{n_{sr}}^{(n_{sw})} \end{pmatrix} \rightarrow r_{n_{sr}}\right. \tag{21}$$

where w_i^j indicates the i-th step of the wheel profile that evolves on j-th step of the rail profile r_j (with $0 \leq i \leq n_{sw} - 1$ and $0 \leq j \leq n_{sr} - 1$). The initial profiles w_0^j are always the same for each j and correspond to the unworn wheel profile (ORE S1002).

Initially the wheel (starting from the unworn profile w_0^0) evolves on the unworn rail profile r_0 to produce the discrete wheel profiles $w_0^0, w_1^0, ..., w_{n_{sw}}^0$ (step $p_{1,1}$). Then the virtual rail profiles $r_1^{(i+1)}$, obtained by means of the simulations (w_i^0, r_0), are arithmetically averaged so as to get the update rail profile r_1 (step $p_{1,2}$). This procedure can be repeated n_{sr} times in order to perform all the rail discrete steps (up to the step $p_{n_{sr},2}$).

The computational effort required by the simulation strategy is the following:

(a) in the wheel wear study, for each update of the rail profile r_j (n_{sr} updates), the whole wheel wear loop w_i^j (n_{sw} steps of simulation) is simulated. The computational effort results of $n_{sw} \times n_{sr} = 100$ steps both for the dynamic analysis (in Simpack Rail) and for the wear model necessary to calculate the removed material on the wheel (in Matlab).
(b) in the rail wear study, the dynamic analyses are the same of the previous case because for each rail step the wheel profiles w_i^j are simulated on r_j in order to obtain $r_j^{(i+1)}$ and thus the updated rail profile r_{j+1} by means of an arithmetic mean. Therefore, no additional dynamical analyses are needed. In this case, only the wear model steps $n_{sw} \times n_{sr} = 100$ must be simulated so as to get the removed material on the rail.

6.2. *Complete railway Aosta-Pre Saint Didier line results*

In this section, the results obtained studying the whole Aosta-Pre Saint Didier line will be presented and compared with the experimental data.

6.2.1. *Evolution of wear control parameters*

In this section, the evolution of the wheel reference quotas numerically evaluated by means of the wear model (flange thickness (FT), FH and flange steepness (QR)) will be compared with the experimental data concerning the three *DMUs Aln 501 Minuetto* vehicles. Furthermore, the rail reference quota QM evolution will be shown and compared with the criterion present in the literature based on the total tonnage burden on the track [21].

The progress of FT dimension, for the n_{sr} discrete step of the rail, is shown in Figure 5 as a function of the mileage; as it can be seen, the decrease of the dimension is almost linear with the travelled distance except in the first phases, where the profiles are still not conformal enough. The FH quota progress is represented in Figure 6 and shows that, due to the high sharpness of the considered track and to the few kilometres travelled, the wheel wear is mainly localized on the flange rather than on the tread; therefore the FH remains near constant in agreement with experimental data. The range of variation of FH is quite small, and it is difficult to recognize a trend for the considered variable; in particular, further experimental analysis characterized by a longer travelled distance and a higher wheel thread wear would be necessary. Since the considered test case (Minuetto vehicle operating on the Aosta-Pre Saint Didier line) is very critical from the wear viewpoint, the flange wear is often more severe than the tread one, leading to an increase of the FH quota and to high climbing and derailment risk. This is especially true during the first phases of the rail life when the contact between wheel and rail is still far from

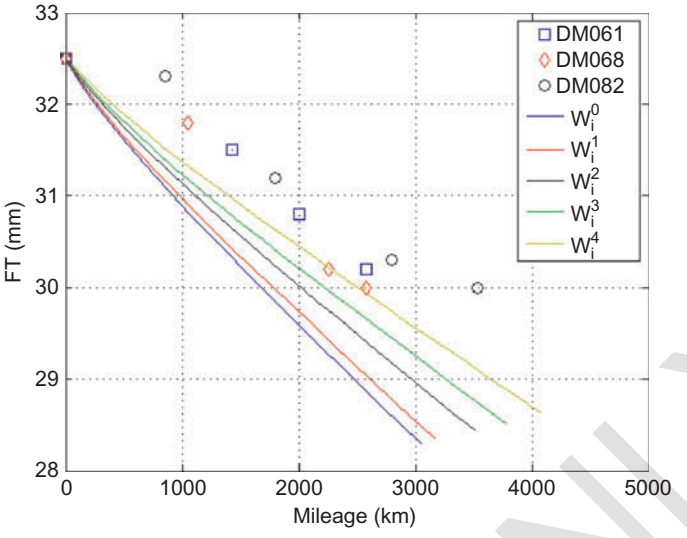

Figure 5. Complete railway line: FT dimension progress.

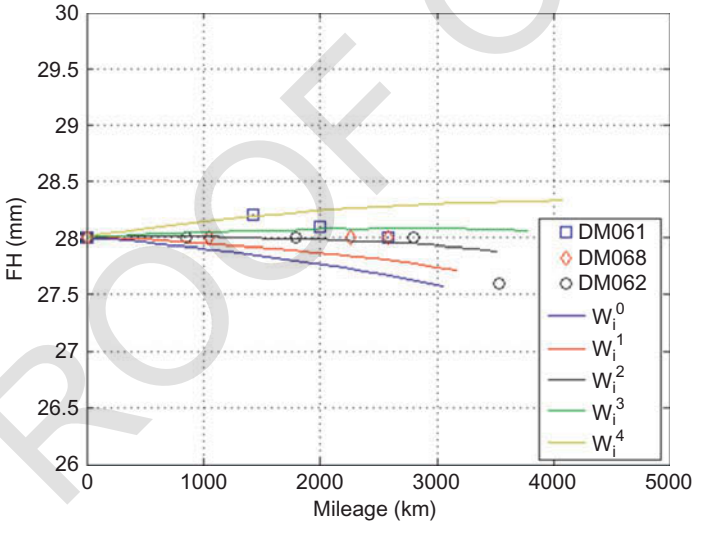

Figure 6. Complete railway line: FH dimension progress.

conformity. The QR trend is shown in Figure 7; also QR decreases almost linearly except in the first phases, leading to an increase of the conicity of the flange.

The simulated QR decreases a little more slowly than the measured one. The differences between the measured QR evolution and the simulated one could depend on the linear filters used in the profiles update procedure to erase the numerical noise from the profile shapes. For this reason, the removed material may be spread also in zones where wheel-rail contact points are not really present. Obviously this effect of the numerical filters has to be reduced as much as possible not to worsen the model accuracy. Moreover,

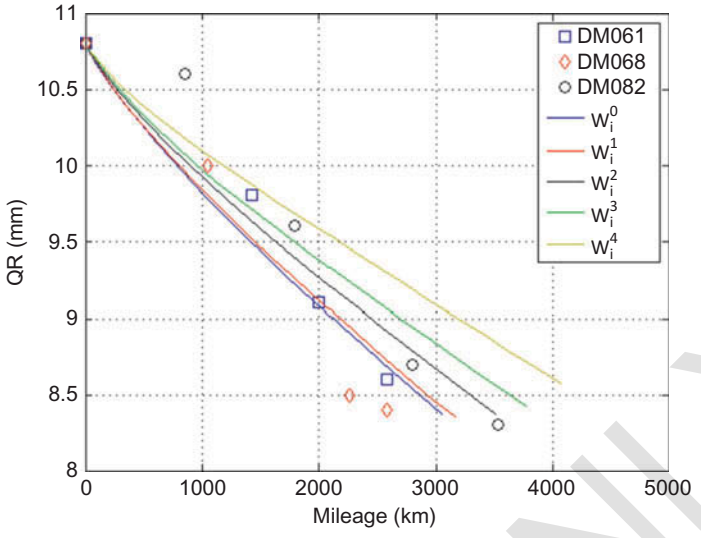

Figure 7. Complete railway line: QR dimension progress.

other physical wear phenomena currently not considered in the proposed model such as the rolling contact fatigue (RCF) and plastic wear could influence the QR trend.

Finally the evolution of the wheel control parameters remains qualitatively similar as the rail wear raises, with a slight increase of all the quotas that indicates a shift of the material removed towards the wheel tread, because of the more and more conformal contact. In Table 6, the total mileages travelled by the vehicle for each rail step n_{sr} are showed.

The QM evolution for the analysis of the rail wear is presented in Figure 8 and shows the almost linear dependence between the rail wear and the total tonnage burden on the track. The amount of removed material on the rail head, equal to 2.97 mm, is in agreement with the criterion present in the literature (1 mm on the rail head height every 100 Mt of accumulated tonnage); the total vehicle number evolving on the track during the whole simulation procedure ($N_{tot} = 2,957,850$) corresponds to a tonnage of $M_{tot} = N_{tot} * M_v = 310$ Mt. (The vehicle mass is $M_v = 104,700$ kg (see Table 2).)

In Figure 9, the evolution of the km_{step} as a function of the wheel discrete step number n_{sw} is shown (for brevity, only the km_{step} related to the first and the latter rail step are presented). Related to the first rail step r_0, the lower km_{step} values and their particular increasing trend in the first wheel steps indicate the higher wear rate due to the initial non-conformal contact characterizing the coupling between the new ORE S1002 wheel profile

Table 6. Evolution of the total mileage km_{tot}.

	km_{tot} (km)
km_{tot}^0	3047
km_{tot}^1	3163
km_{tot}^2	3515
km_{tot}^3	3772
km_{tot}^4	4080

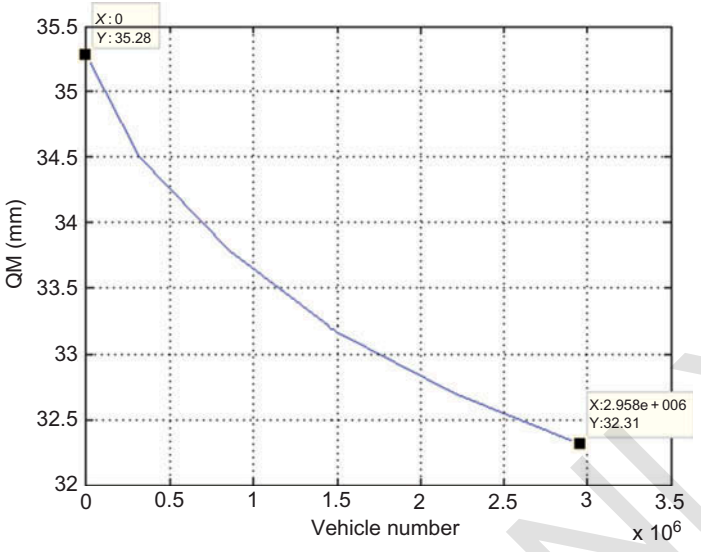

Figure 8. Complete railway line: QM dimension progress.

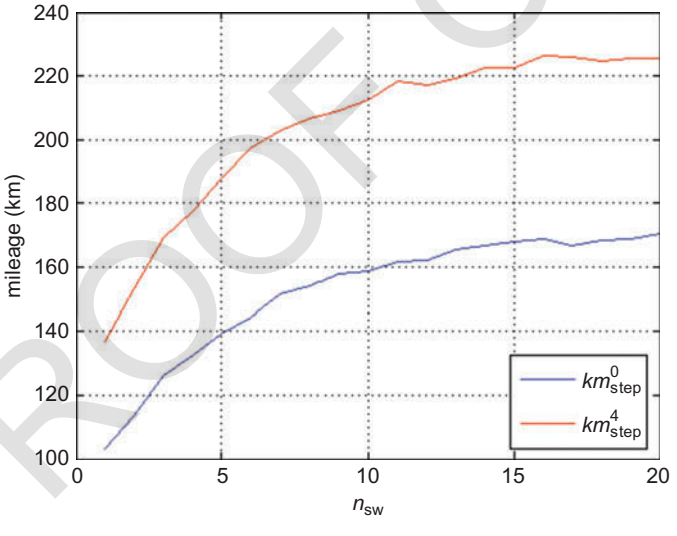

Figure 9. Complete railway line: evolution of the km_{step}.

and the rail profile UIC60 with laying angle equal to 1/20; the almost constant values in the latter steps (combined with higher km_{step} values) show at the same time the achievement of a more and more conformal contact as the wheel wear increases. Considering the latter rail step r_4, the same curve trend can be seen but characterized by higher km_{step} values because of the worn rail profile that leads to an initial more conformal contact than the previous case. In Figure 10, the evolution of the N_{step} as a function of the rail discrete number n_{sr} shows that the considerations related to the variation of the contact conformity hold also for the rail wear evolution.

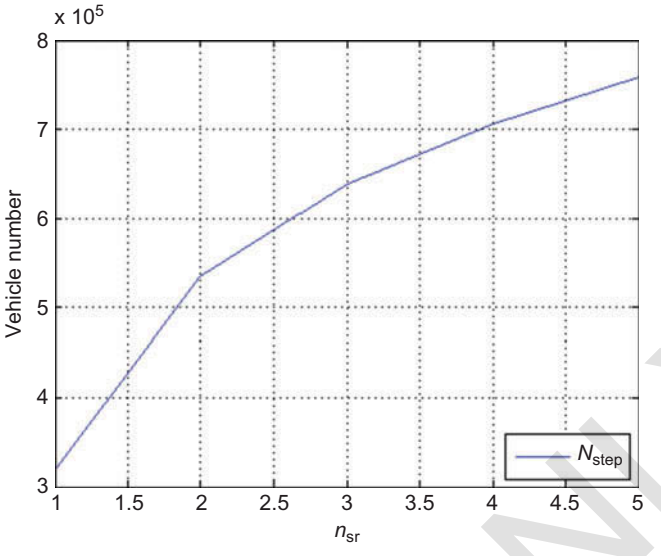

Figure 10. Complete railway line: evolution of the N_{step}.

6.2.2. *Evolution of the wheel and rail profile*

The wear evolution on the wheel profiles evolving on different rail steps is presented in Figures 11 and 12 (for reasons of brevity, only the profiles evolution related to the first and the last rail steps are represented). As stated previously, the wheel profile evolution is described by means of $n_{sw} = 20$ steps, and the threshold on the removed material for each step D^{w}_{step} has been chosen equal to 0.2 mm. Figures 11 and 12 show the main localization

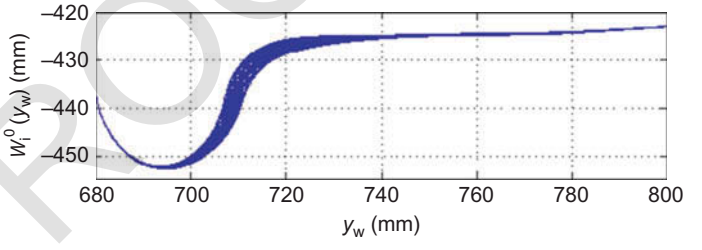

Figure 11. Complete railway line: w_i^0 profile evolution.

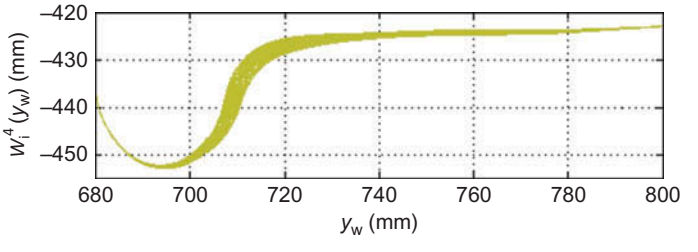

Figure 12. Complete railway line: w_i^4 profile evolution.

of the material removed on the wheel flange due to the quite sharp curves that characterize the Aosta-Pre Saint Didier line. As it can be seen, the flange wear extends right to the top; this is not a physical behaviour but a numerical effect due to the profiles update procedure that uses linear filters to erase the numerical noise and short spatial wavelengths from the profile shapes. (These phenomena are not physical and may cause several problems to the contact models during the dynamical simulations.) For this reason, the removed material may be spread also in zones where wheel-rail contact points are not really present. Obviously this effect of the numerical filters has to be reduced as much as possible not to worsen the model accuracy.

Figures 13 and 14 show the cumulative distributions of removed material in vertical direction z_w on the wheel profile at the first and the last rail step $\sigma_{w_{Kw}}{}^{0}(y_w) = \sum_{i=1}^{Kw} \sigma_i^{w0}(y_w)$ and $\sigma_{w_{Kw}}{}^{n_{sr}-1}(y_w) = \sum_{i=1}^{Kw} \sigma_i^{wn_{sr}-1}(y_w)$ as a function of y_w ($1 \leq Kw \leq n_{sw}$), where $\sigma_i^{wj}(y_w)$ is the removed material between two subsequent discrete steps of the wheel profile evolution (the $i-th$ and the $(i-1)-th$ wheel discrete steps) at the $j-th$ rail step ($0 \leq j \leq n_{sr}-1$) (for reasons of brevity, only the distributions characterized by $Kw = 1, 10, n_{\mathrm{sw}}$ are represented). It can be seen a shift of the material removed towards the wheel tread as the wheel is coupled with more and more worn rail profile due to the achievement of the conformal contact in the wheel-rail pairs.

In Figure 15, the evolution of the rail profile is shown, described by means of $n_{\mathrm{sr}} = 5$ discrete step and with the threshold on the removed material for each step D^r_{step} equal to 0.8 mm.

The average operations on all the N_c curves and on the inner and outer sides of the rail (necessary, at this phase of the activity, to obtain a single rail profile as output of the wear model) lead approximately to the same rail head and gauge corner wear rates. In fact, the rail head wear is more relevant on the inner rail while the gauge corner wear becomes prevalent on the outer one; therefore the average operations could lead to comparable wear effects both on the rail head and on the gauge corner rail. Furthermore, the gauge corner wear extends below possible contact point locations: this is mainly due to the linear filters used in the profile update procedure to erase the numerical noise from the profile shapes and to other physical wear phenomena currently not considered in the proposed model such as the RCF and plastic wear.

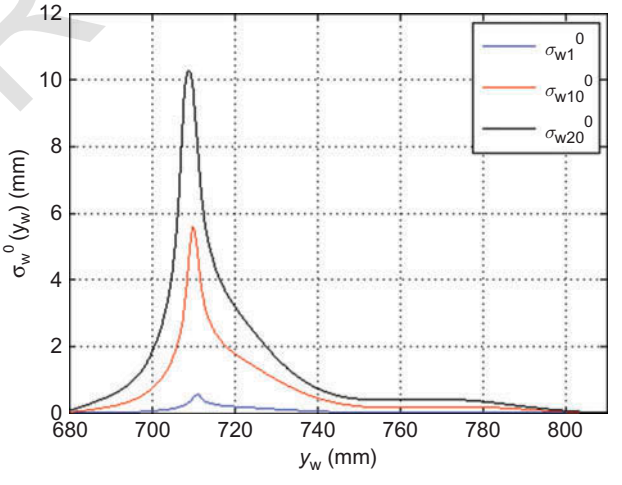

Figure 13. Complete railway line: cumulative distributions $\sigma_{wi}{}^0$ of the removed wheel material.

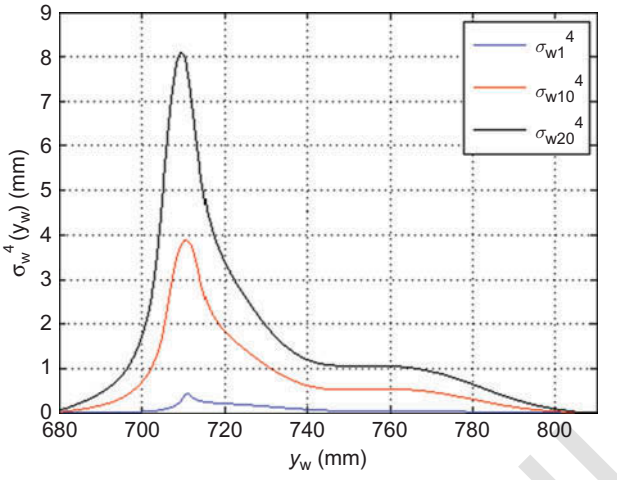

Figure 14. Complete railway line: cumulative distributions σ_{wi}^4 of the removed wheel material.

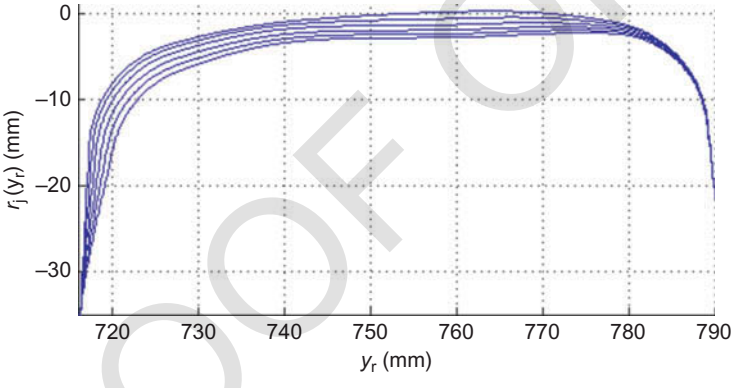

Figure 15. Complete railway line: rail profile evolution.

6.3. *Statistical analysis results*

In this section, the results obtained with the statistical analysis approach will be presented. For this pourpose, a suitable value of the n_{class} parameter has to be supposed. For the Aosta-Pre Saint Didier line, the value $n_{class} = 10$, as will be shown in the following, represents a good compromise among track description, result accuracy and computational effort; in fact a n_{class} too high would increase the result accuracy but would increase the computational time too and would lead to a high number of curve classes quite difficult to be statistically treated.

6.3.1. *Evolution of wear control parameters*

Figures 16–19 present the evolution of the wear control parameters. It can be seen the same qualitatively trend obtained with the complex railway approach both related to the comformity considerations and the localization of the worn material on the wheel flange.

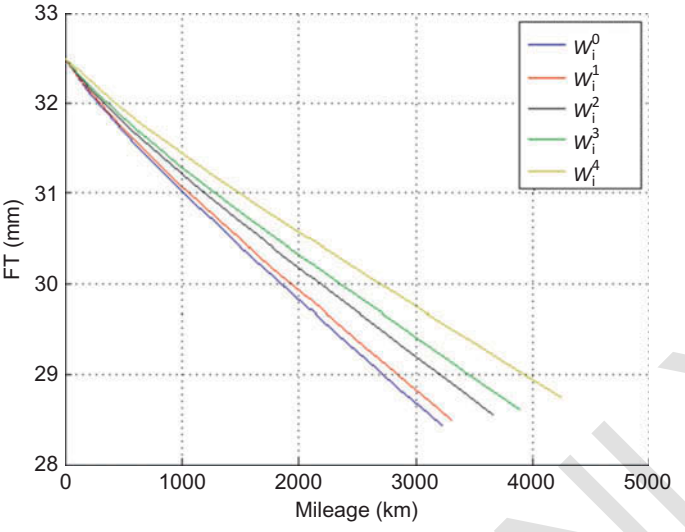

Figure 16. Statistical analysis approach: FT dimension progress.

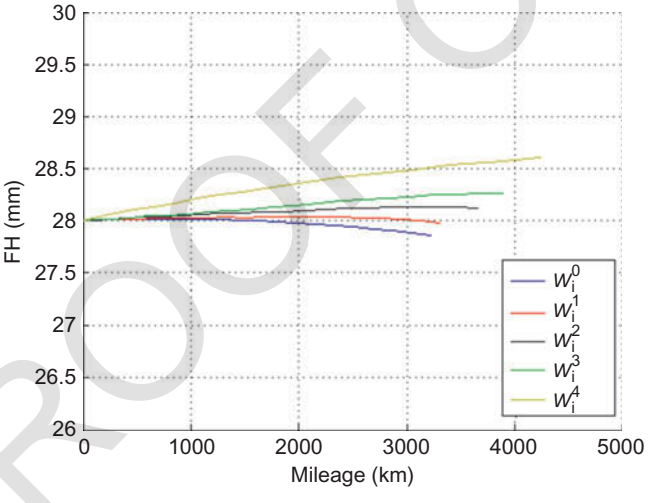

Figure 17. Statistical analysis approach: FH dimension progress.

In Table 7, it can be seen the total mileage travelled by the vehicle for each rail step n_{sr}. QM progress leads to a reduction of the rail head height of 3.28 mm in agreement with the criterion present in the literature (1 mm on the rail head height every 100 Mt of accumulated tonnage); in fact, the total vehicle number evolving on the curved track of the statistical description during the whole simulation ($N_{tot} = 3,076,200$) corresponds to a tonnage of $M_{tot} = N_{tot} * M_v = 322$ Mt.

The evolution of the km_{step} and N_{step} as a function of the wheel and rail step numbers n_{sw} and n_{sr}, respectively, can be seen in Figures 20 and 21 and shows that the considerations related to the variation of the contact conditions due to the increase of the rail wear (i.e. non-conformal and conformal contact) hold also in this case.

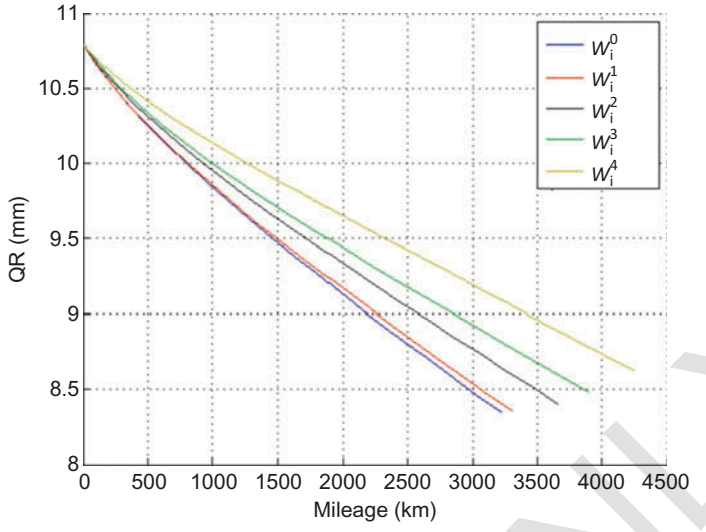

Figure 18. Statistical analysis approach: QR dimension progress.

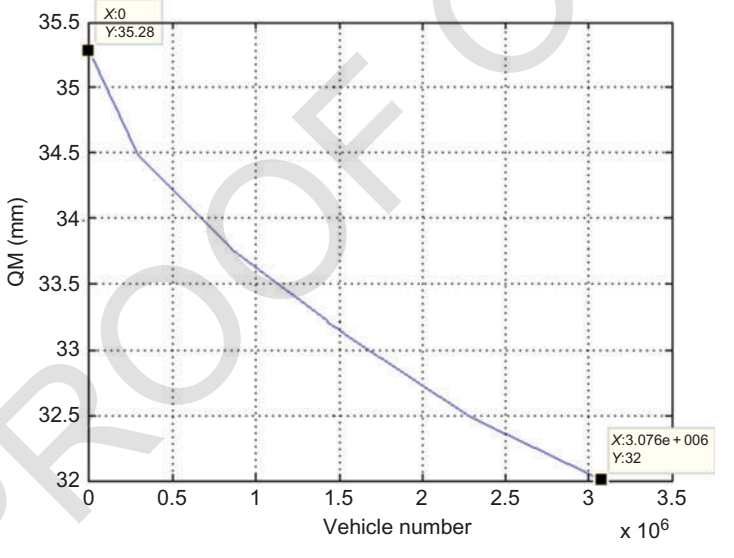

Figure 19. Statistical analysis approach: QM dimension progress.

Table 7. Evolution of the total mileage km_{tot}.

	km_{tot} (km)
km_{tot}^0	3219
km_{tot}^1	3306
km_{tot}^2	3659
km_{tot}^3	3893
km_{tot}^4	4244

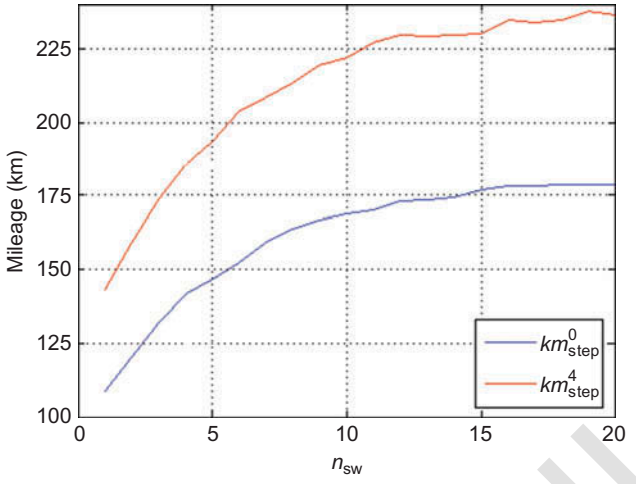

Figure 20. Statistical analysis approach: evolution of the km_{step}.

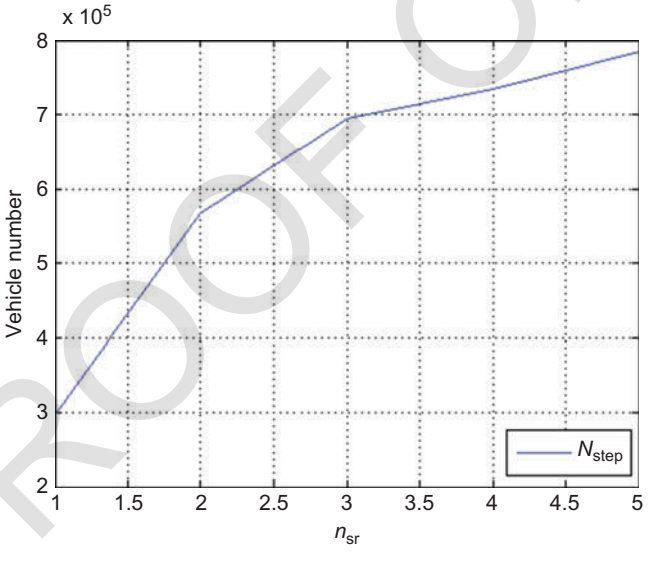

Figure 21. Statistical analysis approach: evolution of the N_{step}.

6.3.2. *Evolution of the wheel and rail profile*

As can be seen in Figures 22–25, the evolution of the wheel profile and the cumulative distributions of removed material is qualitatively in agreement with the complete railway approach and the same considerations of Section 6.2.2 are valid (for reasons of brevity, only the figures referred to the first and the last rail steps are presented). Finally, the evolution of the rail profile evolution obtained with the statistical approach is presented in Figure 26.

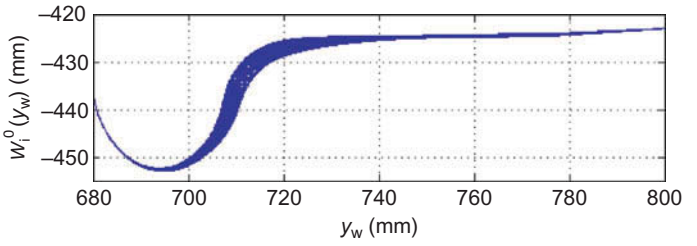

Figure 22. Statistical analysis approach: w_i^0 profile evolution.

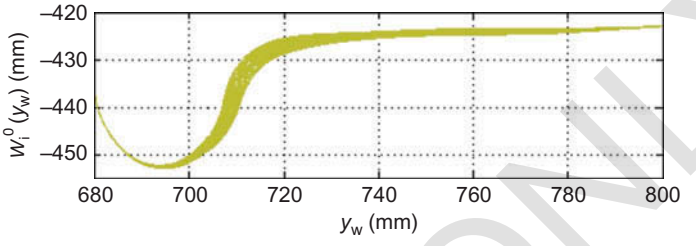

Figure 23. Statistical analysis approach: w_i^4 profile evolution.

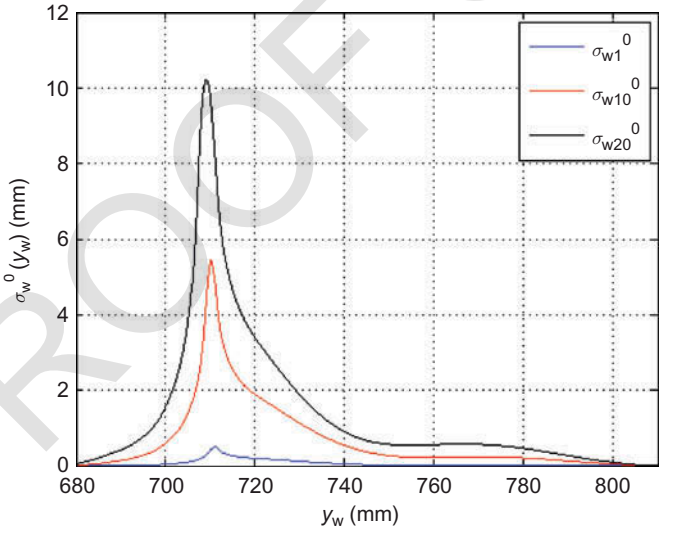

Figure 24. Statistical analysis approach: cumulative distributions $\sigma_{wi}{}^0$ of the removed wheel material.

6.4. *Comparison between the complete railway line and statistical analysis*

In this section, a quantitatively comparison between the results obtained with the complete railway line and the statistical approach with $n_{\text{class}} = 10$ will be carried out. In Tables 8–10, the final values of the wheel reference dimensions for each rail step n_{sw} are presented. The increase of FH as the rail profile is more and more worn, together with

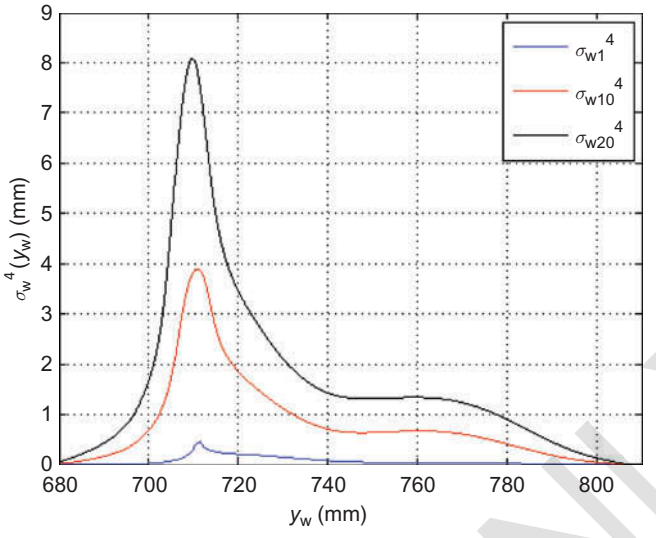

Figure 25. Statistical analysis approach: cumulative distributions $\sigma_{wi}{}^4$ of the removed wheel material.

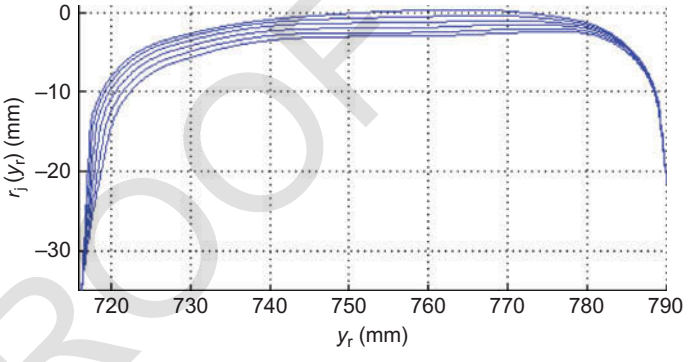

Figure 26. Statistical analysis approach: rail profile evolution.

Table 8. Evolution of the FH quota.

Complete railway		Statistical description $n_{\text{class}} = 10$	
	FH (mm)	FH (mm)	e (%)
km_{tot}^0	27.57	27.86	1.0
km_{tot}^1	27.73	27.98	0.9
km_{tot}^2	27.89	28.12	0.8
km_{tot}^3	28.07	28.27	0.7
km_{tot}^4	28.33	28.60	1.0

Table 9. Evolution of the FT quota.

Complete railway		Statistical description $n_{class} = 10$	
	FT (mm)	FT (mm)	e (%)
km^0_{tot}	28.30	28.43	0.5
km^1_{tot}	28.36	28.50	0.5
km^2_{tot}	28.44	28.56	0.4
km^3_{tot}	28.52	28.62	0.4
km^4_{tot}	28.63	28.75	0.4

Table 10. Evolution of the QR quota.

Complete railway		Statistical description $n_{class} = 10$	
	QR (mm)	QR (mm)	e (%)
km^0_{tot}	8.38	8.35	0.4
km^1_{tot}	8.35	8.36	0.1
km^2_{tot}	8.37	8.41	0.5
km^3_{tot}	8.43	8.48	0.6
km^4_{tot}	8.57	8.63	0.7

the increase of FT, indicates a shift of the material removed towards the wheel tread due to the variations of the contact conditions as explained in previous sections. The reference dimension comparison shows a good consistency between the two investigation approaches with a maximum error equal to $e = 1.0\%$.

Table 11 displays the evolution of the total mileage km_{tot} as a function of the rail step n_{sw} and shows a good consistency between the two considered procedures: the increase of the mileage travelled by the vehicle, as the rail profile is more and more worn, indicates a decrease of the wear rate explained by a better conformity between wheel and rail surfaces.

Finally the comparison of the parameters QM and N_{tot} needed to evaluate the rail wear provided the following results ($n_{class} = 10$): $QM = 32.31$ mm and $N_{tot} = 2,957,850$ for the complete railway and $QM = 32.11$ mm ($e = 0.6\%$)) and $N_{tot} = 3,076,200$ ($e = 4.0\%$)) for the statistical description.

Table 11. Evolution of the total mileage km_{tot}.

Complete railway		Statistical description $n_{class} = 10$	
	km_{tot} (km)	km_{tot} (km)	e (%)
km^0_{tot}	3047	3219	5.6
km^1_{tot}	3163	3306	4.5
km^2_{tot}	3515	3659	4.1
km^3_{tot}	3772	3893	3.2
km^4_{tot}	4080	4244	4.0

6.5. *Sensibility analysis of the statistical approach*

In this section, a sensibility analysis of the statistical approach with respect to the class number n_{class}, i.e. the most important parameter of the track discretization, will be presented. The variation range studied is $n_{class} = 4 \div 10$. By analysing the data relative to the wheel presented in Table 12, for each value of n_{class} investigated, the trend of the wheel parameters shows an increase in both of the wheel flange dimensions according to the variation of the contact conditions explained in the previous sections (see Section 6.2–6.4). Analogously the km_{tot} evolution trend is the same for each of the statistical analysis considered, and also the mileage increases as the rail wear increases, indicating the more

Table 12. Evolution of the wheel control parameters (quotas and km_{tot}).

Statistical Description		FH (mm)	e (%)	FT (mm)	e (%)	QR (mm)	e (%)	km_{tot} (km)	e (%)
$n_{class} = 4$	km^0_{tot}	26.99	2.1	28.02	1.0	8.29	1.0	3775	23.9
	km^1_{tot}	27.12	2.2	28.16	0.7	8.25	1.2	3967	25.4
	km^2_{tot}	27.26	2.3	28.19	0.9	8.28	1.1	4267	21.4
	km^3_{tot}	27.49	2.1	28.26	0.9	8.35	1.0	4521	19.9
	km^4_{tot}	27.71	2.2	28.35	1.0	8.47	1.2	4793	17.5
$n_{class} = 5$	km^0_{tot}	27.02	2.0	28.03	1.0	8.31	0.9	3713	21.9
	km^1_{tot}	27.16	2.0	28.16	0.7	8.27	0.9	3877	22.6
	km^2_{tot}	27.31	2.1	28.20	0.9	8.29	1.0	4129	17.5
	km^3_{tot}	27.54	1.9	28.27	0.9	8.35	0.9	4397	16.6
	km^4_{tot}	27.75	2.0	28.36	0.9	8.48	1.1	4688	14.9
$n_{class} = 6$	km^0_{tot}	27.08	1.7	28.06	0.8	8.31	0.8	3620	18.8
	km^1_{tot}	27.24	1.7	28.18	0.6	8.28	0.9	3743	18.5
	km^2_{tot}	27.40	1.8	28.23	0.7	8.29	0.9	4038	14.9
	km^3_{tot}	27.62	1.6	28.31	0.8	8.36	0.9	4237	12.3
	km^4_{tot}	27.83	1.8	28.40	0.8	8.48	1.1	4569	12.0
$n_{class} = 7$	km^0_{tot}	27.11	1.7	28.09	0.7	8.31	0.8	3535	16.0
	km^1_{tot}	27.26	1.7	28.19	0.6	8.29	0.8	3676	16.2
	km^2_{tot}	27.43	1.7	28.25	0.7	8.30	0.9	3984	13.3
	km^3_{tot}	27.65	1.5	28.33	0.6	8.36	0.8	4172	10.6
	km^4_{tot}	27.85	1.7	28.42	0.7	8.48	1.0	4503	10.4
$n_{class} = 8$	km^0_{tot}	27.14	1.6	28.10	0.7	8.33	0.6	3431	12.6
	km^1_{tot}	27.30	1.5	28.19	0.6	8.30	0.5	3529	11.6
	km^2_{tot}	27.47	1.5	28.26	0.6	8.31	0.7	3903	11.0
	km^3_{tot}	27.69	1.3	28.35	0.6	8.37	0.8	4092	8.5
	km^4_{tot}	27.90	1.5	28.44	0.7	8.49	0.9	4445	8.9
$n_{class} = 9$	km^0_{tot}	27.20	1.3	28.13	0.6	8.33	0.6	3308	8.6
	km^1_{tot}	27.37	1.3	28.20	0.6	8.32	0.4	3397	7.4
	km^2_{tot}	27.55	1.2	28.28	0.5	8.31	0.6	3777	7.4
	km^3_{tot}	27.77	1.1	28.38	0.5	8.37	0.7	4011	6.4
	km^4_{tot}	27.97	1.3	28.47	0.6	8.50	0.8	4343	6.4
$n_{class} = 10$	km^0_{tot}	27.86	1.0	28.43	0.5	8.35	0.4	3219	5.6
	km^1_{tot}	27.98	0.9	28.50	0.5	8.36	0.1	3306	4.5
	km^2_{tot}	28.12	0.8	28.56	0.4	8.41	0.5	3659	4.1
	km^3_{tot}	28.27	0.7	28.62	0.4	8.48	0.6	3893	3.2
	km^4_{tot}	28.60	1.0	28.75	0.4	8.63	0.7	4244	4.0

Table 13. Evolution of the rail control parameters (QM quota and N_{tot}).

Statistical Description	QM (mm)	e (%)	N_{tot}	e (%)
$n_{class} = 4$	31.58	2.3	3,797,900	28.4
$n_{class} = 5$	31.63	2.1	3,641,100	23.1
$n_{class} = 6$	31.69	1.9	3,543,500	19.8
$n_{class} = 7$	31.75	1.7	3,398,600	14.9
$n_{class} = 8$	31.83	1.5	3,309,800	11.9
$n_{class} = 9$	31.86	1.4	3,188,600	7.8
$n_{class} = 10$	32.00	1.0	3,076,200	4.0

and more conformal contact between wheel and rail surfaces. The error e presented in Table 12 is referred to the complete railway approach (see Section 6.2) and shows less and less consistency between the results of the whole railway approach and the statistical analysis as the n_{class} parameter decreases: in particular, small n_{class} values corresponding to a rough discretization of the track, lead to an important underestimation of the removed material highlighted by the increasing mileage travelled. The less accuracy of the model and the underestimation of the worn material as the track description is more and more rough are found also by analysing the rail control parameter and the number of the train evolving on the track (see Table 13).

6.6. *Computational effort comparison*

In this section, the comparison between the computational load required by the different approaches considered in this work, i.e. the complete railway line and all the analysed statistical track descriptions ($n_{class} = 4 \div 10$), will be performed.

The characteristics of the processor and the main numerical parameters relative to the integrator used for the dynamical simulations are briefly reported in Table 14. During the dynamical simulations, a fixed step ODE integrator has been used to have the better numerical strength (fixed and variable step solvers have been tested and because of the problem stiffness, both ones provided comparable performance in terms of accuracy and numerical efficiency). In fact, considering the remarkable simulation times and memory consumption, it was important to reduce the risk of slowing down and stopping of the solver (and thus of the simulation) due to the problem stiffness. This risk is quite high in this kind of problems, even if suitable stiff variable step solvers are used. At the same time, the capability of correctly following the non-linear wheel and rail wear evolution is

Table 14. Processor and integrator data.

Processor	INTEL Xeon CPU X5560 2.80 GHz 24 GB RAM	
Integrator	Type	ODE5
	Algorithm	Dormand-Prince
	Order	5
	Step type	fixed
	Step size	10^{-4} s

Table 15. Computational time.

Railway approach		Computational time						
		Wheel wear evaluation			Rail wear evaluation			Total simulation time
		t_{wd}	t_{ww}	t_{wt}	t_{rd}	t_{rw}	t_{rt}	t_T
Complete track		4 d 12 min	1 d 38 min	5 d 50 min	3 d 12 h	1 d 8 h 40 min	4 d 20 h 40 min	24 d 7 h 20 min
Statistical analysis	$n_{class} = 4$	8 min	4 min	12 min	2 h 40 min	1 h 20 min	4 h	20 h
	$n_{class} = 5$	11 min	4 min	15 min	3 h 40 min	1 h 20 min	5 h	1 d 1 h
	$n_{class} = 6$	13 min	6 min	19 min	4 h 20 min	2 h	6 h 20 min	1 d 7 h 40 min
	$n_{class} = 7$	15 min	7 min	22 min	5 h	2 h 20 min	7 h 20 min	1 d 12 h 40 min
	$n_{class} = 8$	18 min	7 min	25 min	6 h	2 h 20 min	8 h 20 min	1 d 16 h 40 min
	$n_{class} = 9$	21 min	9 min	30 min	7 h	3 h	10 h	2 d 2 h
	$n_{class} = 10$	24 min	10 min	34 min	8 h	3 h 20 min	11 h 20 min	2 d 8 h 40 min

assured by the innovative update procedure of the profiles and it is not influenced by the considered solver type.

The mean computational times relative to each discrete step of the whole model loop (for the wheel and for the rail wear evaluation) are schematically summarized in Table 15 both for the complete railway line and for the statistical descriptions.

The mean computational times related to the discrete steps of the whole wear model corresponding to one complete loop described in Figure 1 (t_{wt}, t_{rt} for wheel and rail, respectively) are subdivided in dynamical simulation times (t_{wd}, t_{rd} for wheel and rail, respectively) and wear simulation times (t_{ww}, t_{rw} for wheel and rail, respectively). Obviously for all the rail computation times (t_{rt}, t_{rd}, t_{rw}), the relations $t_{rt} = n_{sw} * t_{wt}$, $t_{rd} = n_{sw} * t_{wd}$ and $t_{rw} = n_{sw} * t_{ww}$ hold, and the total simulation time is $t_T = n_{sr} * t_{rt}$, where $n_{sw} = 20$ and $n_{sr} = 5$ are the wheel and rail discrete step number introduced in the previous sections.

The huge computational effort that affects the complete railway line simulation (more than 24 days for a complete simulation loop) makes this approach hardly feasible to the wear evolution studies typical of the railway field. On the contrary, the statistical track description (see Tables 12, 13 and 15) shows a high saving of computational load and at the same time not an excessive loss of model accuracy; in particular with a number of curve class $n_{class} = 10$, wear evaluation results are qualitatively and quantitatively in agreement with the complete line approach (a maximum error $e \simeq 5\%$ on the mileage travelled by the vehicle has been found). In conclusion, the innovative wear model developed for the study of complex railway networks using a statistical track description approach is capable of simulating the wear evolution both on the wheel and on the rail surfaces with reasonable computational time and leads to a good result consistency with respect to the considered experimental data.

AQ9

7. Conclusions

In the present work, the authors introduce a complete model for wheel and rail wear prediction in railway applications expressly conceived (in collaboration with our industrial partners, which provided technical and experimental data) for complex railway networks where the complete simulation of the vehicle running on the entire line is not practicable due to the high computational load required. The entire model has been validated on a critical operating setting in terms of wear in Italian railways: the ALSTOM *DMU Aln 501 Minuetto* operated on the Aosta-Pre Saint Didier railway line. The results coming from the innovative model have been compared both with the outputs from the complete railway network simulations and with the experimental data.

Future developments will consist on further experimental data (measurements performed on other railway track with an higher mileage than the Aosta-Pre Saint Didier line) always provided by our partners and referred to deep wear on wheel (especially on the wheel tread) and rail. The new and more extensive experimental campaign will allow the direct measurement of the rail wear (rail head wear, rail side wear and complete rail profile) and a further validation of the developed wear model. Other simulations will be performed to further validate the entire model and to enhance the investigation on the statistical approach. In such a way, further sensitivity study of the statistical analysis (mainly correlated with traction and brake forces, impulsive events such as transit on turnouts and weather conditions) will be carried out.

References

[1] Malvezzi M, Meli E, Rindi A, Falomi S. Determination of wheel-rail contact points with semianalytic method. Multibody Syst Dyn. 2008;20:327–358.
[2] Auciello J, Meli E, Falomi S, Malvezzi M. Dynamic simulation of railway vehicles: wheel/rail contact analysis. Vehicle Syst Dyn. 2009;47:867–899.
[3] Kalker JJ. Three-dimensional elastic bodies in rolling contact. Norwell, MA: Kluwer Academic Publishers; 1990.
[4] Kalker JJ. Survey of wheel-rail rolling contact theory. Vehicle Syst Dyn. 1979;8:317–358.
[5] Hertz H. The contact of elastic solids. J Reine Angew Math. 1881;92:156–171.
[6] Braghin F, Lewis R, Dwyer-Joyce RS, Bruni S. A mathematical model to predict railway wheel profile evolution due to wear. Wear. 2006;261:1253–1264.
[7] Official Site of the INTEC GmbH. Berlin, Germany: 2012. Available from:http://www.simpack.com.
[8] Krause H, Poll G. Verschleiss bei gleitender und waelzender Relativbewegung. Tribologie und Schmierungstechnik. 1984;31:209–214.
[9] Pombo J, Ambrosio J, Pereira M, Lewis R, Dwyer-Joyce R, Ariaudo C, Kuka N. A study on wear evaluation of railway wheels based on multibody dynamics and wear computation. Multibody Syst Dyn. 2010;24:347–366.
[10] Zobory I. Prediction of wheel/rail profile wear. Vehicle Syst Dyn. 1997;28:221–259.
[11] Jendel T, Berg M. Prediction of wheel profile wear. Suppl. Vehicle Syst Dyn. 2002;37:502–513.
[12] Enblom R, Berg M. Simulation of railway wheel profile development due to wear influence of disc braking and contact environment. Wear. 2005;258:1055–1063.
[13] Ignesti M, Innocenti A, Marini L, Meli E, Rindi A. Development of a wear model for the wheel profile optimisation on railway vehicles. Vehicle Syst Dyn. 2013;51:1363–1402.
[14] Auciello J, Ignesti M, Malvezzi M, Meli E, Rindi A. Development and validation of a wear model for the analysis of the wheel profile evolution in railway vehicles. Vehicle Syst Dyn. 2012;50:1707–1734.
[15] Ignesti M, Innocenti A, Marini L, Meli E, Rindi A. Development of a model for the simultaneous analysis of wheel and rail wear in railway systems. Multibody Syst Dyn. 2013;31:191–240.
[16] Ignesti M, Malvezzi M, Marini L, Meli E, Rindi A. Development of a wear model for the prediction of wheel and rail profile evolution in railway systems. Wear. 2012;284–285:1–17.
[17] Ignesti M, Innocenti A, Marini L, Meli L, Rindi A, Toni P. Wheel profile optimization on railway vehicles from the wear viewpoint. Int J Non-Linear Mech. 2013; 53:41–54.
[18] Ignesti M, Innocenti A, Marini L, Meli E, Rindi A. A numerical procedure for the wheel profile optimisation on railway vehicles. J Eng Tribol. 2013;228:206–222.
[19] Pombo J, Ambrosio J, Pereira M, Lewis R, Dwyer-Joyce R, Ariaudo C, Kuka N. Development of a wear prediction tool for steel railway wheels using three alternative wear functions. Wear. 2011;20:327–358.
[20] Enblom R. On simulation of uniform wear and profile evolution in the wheel-rail contact [Ph. D. thesis]. Stockholm: Royal Institute of Technology; 2006.
[21] Esveld C. Modern railway track. Delft: Delft University of Technology; 2001.
[22] Toni P. Ottimizzazione dei profili delle ruote su binario con posa 1/20. Trenitalia S.p.A.; 2010.
[23] Iwnicki S. The Manchester Benchmarks for Rail Vehicle Simulators. Lisse: Swets and Zeitlinger; 1999.
[24] Iwnicki S. Handbook of railway vehicle dynamics. Lisse: Taylor and Francis; 2006.
[25] Antoine JF, Visa C, Sauvey C, Abba G. Approximate analytical model for hertzian elliptical contact problems. J Tribol. 2006;128:660–664.
[26] Kalker JJ. A fast algorithm for the simplified theory of rolling contact. Vehicle Syst Dyn. 1982;11:1–13.
[27] UNI-EN 15313. Railway applications. In-service wheelset operation requirements. In-service and off-vehicle wheelset maintenance. UNI-EN: 2010.
[28] Pearce TG, Sherratt ND. Prediction of wheel profile wear. Wear. 1991;144:343–351